

Democratic and Popular Republic of Algeria
Ministry of Higher Education and Scientific Research



University A. Mira of Bejaia
Faculty of Exact Sciences
Department of Computer Science

MASTER'S THESIS

In
Computer Science

Option
Artificial Intelligence

Theme

A novel U-Net variant with encoder noise injection
for breast tumor segmentation in DCE-MRI

Presented by: Massy Aftis

Defended on June 30th, 2025 before the jury composed of:

Chair	Mrs. Karima Adel	Full Professor	U. A/Mira of Bejaia.
Examinator	Mr. Kamal Amroun	Full Professor	U. A/Mira of Bejaia.
Examinator	Mr. Mohammed Khammari	Associate Professor	U. A/Mira of Bejaia.
Examinator	Mrs. Samira Boukerram	Assistant Professor	U. A/Mira of Bejaia.
Supervisor	Mr. Fatah Bouchebbah	Associate Professor	U. A/Mira of Bejaia.

Bejaia, 2025/2024.

※ *Remerciements* ※

First and foremost, I would like to express my deepest gratitude to Almighty **ALLAH** for granting me the strength, patience, and perseverance to carry out and complete this work. I would like to extend my sincere thanks to my academic supervisor, **Dr. Bouchebbah Fatah**, for his availability, valuable advice, and continuous support throughout this project. His expertise and rigorous guidance greatly contributed to the quality of this work.

I am also truly grateful to **Aïssaoui Sid Ahmed**, PhD student, for his technical support, valuable methodological insights, and kind assistance during the different stages of the project. I warmly thank **all the professors** who have guided, supported, and taught me from the first year of my bachelor's degree to the final year of my Master 2. Their dedication, pedagogical rigor, and commitment were essential to my academic journey.

Finally, I would like to express my appreciation to all those who, directly or indirectly, contributed to the success of this work.

※ *Dedications* ※

To my dear mother and father,

This work is dedicated to you, as a token of my deep gratitude for all the sacrifices you made to give me the best opportunities in life. Your love and unwavering support have been my strength and guiding light throughout this journey.

To my beloved fiancée, **Agnes**,

Thank you for your constant presence, your precious help, your sincere love, and your support during the most challenging times. You have been an invaluable source of inspiration.

To my dear older brothers, **Fares** (from the United States of America) and **Belaïd**,
Thank you for your encouragement, wise advice, and reassuring presence—even from afar. You have always believed in me.

To my little brother, **Yacine**,

Your joy, energy, and affection were a true source of comfort. Thank you for always being there in your own special way.

To my grandmother,

Your prayers, love, and kind words have always given me strength and peace. Thank you for being a pillar in my life.

To all of you,

Thank you for making this journey more meaningful, stronger, and unforgettable. This work is also yours.

Aftis Massy

Contents

Contents	i
Table of figures	iii
Liste of tables	v
General introduction	2
0.1 Scientific context	2
0.2 Addressed problematic	2
0.3 Aimed objectives and research methodology	3
0.4 Organization of the manuscript	3
1 General overview of breast cancer and image segmentation	5
1.1 Introduction	5
1.2 Anatomy and epidemiology	6
1.2.1 Normal anatomy of the breast	6
1.2.2 Breast tumor	7
1.2.3 Classification of breast tumors	8
1.2.4 Statistics on breast cancer	9
1.3 Biomedical imaging for breast cancer screening	11
1.3.1 Mammography	12
1.3.2 Ultrasonography	13
1.3.3 Computed Tomography (CT)	13
1.3.4 Positron Emission Tomography (PET)	13
1.3.5 Magnetic Resonance Imaging (MRI)	14
1.4 Breast cancer treatment	16
1.4.1 Lumpectomy	16
1.4.2 Mastectomy	16
1.4.3 Chemotherapy	17
1.5 Image segmentation: principles and methods	17
1.5.1 Image processing	17
1.5.2 Deep learning for image segmentation	21

1.6	Conclusion	26
2	State-of-the-art on DCE-MRI breast tumor segmentation	27
2.1	Introduction	27
2.2	Breast DCE-MRI and tumor segmentation	28
2.2.1	Analysis of DCE-MRI images to diagnose breast tumors	28
2.2.2	Importance of DCE-MRI breast tumor segmentation	30
2.2.3	Challenge of breast DCE-MRI images segmentation for accurate extraction of tumors	30
2.3	Description of related work	32
2.3.1	Multiparametric data-driven DCE-MRI breast tumor segmentation methods	33
2.3.2	Uniparametric data-driven DCE-MRI breast tumor segmentation methods	36
2.4	Comparison of the reviewed methods	39
2.5	Synthesis and insights	40
2.6	Conclusion	42
3	RicIU-Net: Rician noise injection in the U-Net Encoder for breast DCE-MRI tumor segmentation	43
3.1	Introduction	43
3.2	Prior work on noise injection as an augmentation technique	44
3.2.1	Description of existing work	44
3.2.2	Gap in the literature and motivation	44
3.3	Rician noise in breast DCE-MRI: Characteristics and impact	45
3.3.1	Rician noise	45
3.3.2	Detrimental effects of Rician noise on breast MRI images	46
3.4	Proposed model: RicIU-Net	46
3.4.1	Feature-space Rician noise injection	47
3.4.2	Rationale for feature-space noise injection	47
3.4.3	Motivation for Encoder-only noise injection	48
3.4.4	RicIU-Net <i>vs.</i> baseline U-Net: Expected improvements	48
3.5	Implementation and evaluation	49
3.5.1	Experimental dataset	49
3.5.2	Development environment and tools	50
3.5.3	RicIU-Net training and validation	51
3.5.4	Evaluation of RicIU-Net and comparison with existing methods	53
3.6	Conclusion	55
	General conclusion	57

List of Figures

1.1	Illustration of a sagittal view of the anatomical structure of the female breast [174] .	6
1.2	Illustration of breast tumor stages according to the TNM system [162]	9
1.3	Pie chart of the global cancer incidence rate in 2022 [165]	10
1.4	Pie chart of the global cancer incidence rate in 2022 [165]	10
1.5	Bar chart of age-standardized incidence and mortality rates by region for female breast cancer in 2022 [165]	11
1.6	Schematic representation of Damadian’s machine [39]	15
1.7	Representation of a modern MRI scanner [76]	15
1.8	Illustration of the modified radical mastectomy [117]	17
1.9	Illustration of an original image and its two possible segmented versions, demonstrating the image segmentation process [84]	18
1.10	Example of a CNN architecture designed for tumor classification [1].	22
1.11	U-Net architecture (example for 32x32 pixels in the lowest resolution) [149]	23
1.12	The Vision Transformer (ViT) architecture, where an input image is split into patches, embedded, and processed through Transformer encoder layers for classification or segmentation [44]	24
1.13	The TransUNet architecture, combining a CNN encoder, Transformer bottleneck, and U-Net-style decoder for medical image segmentation [27]	25
2.1	Illustration of a breast DCE-MRI scanner for cancer diagnosis [188]	29
2.2	An illustration of a benign breast tumor highlighted with a bounded box in DCE-MRI taken from BreastDM dataset [194]	31
2.3	An illustration of a benign breast tumor highlighted with a bounded box in DCE-MRI taken from BreastDM dataset [breastdm2023]	32
2.4	Illustration of a DCE-MRI image presenting different enhanced normal regions	33
2.5	Illustration of the IMIIN network [139]	34
2.6	Modified 3D VGGNet backbone architecture [105]	35
2.7	Mask R-CNN architecture used in the work of Zhang et al. [190]	36
2.8	Illustration of the 3D U-Net convolutional neural network used for segmentation in the work of Hirsch et al. [70]	37
2.9	Architecture of EEU-Net proposed by Rehman et al. [146]	38

3.1	Illustration of the architecture of the proposed RicIU-Net.	49
3.2	Illustration of an implemented part of RicIU-Net’s Encoder.	51
3.3	Illustration of an implemented part of RicIU-Net’s Decoder.	52
3.4	Trend of the DSC for training and validation across epochs.	53
3.5	Trend of the Dice loss for training and validation across epochs.	53
3.6	Example of the segmentation obtained by the proposed RicIU-Net for a small breast tumor.	54
3.7	Example of the segmentation obtained by the proposed RicIU-Net for a medium-sized breast tumor.	55
3.8	Example of the segmentation obtained by the proposed RicIU-Net for a large breast tumor.	55

List of Tables

1.1	Incidence and mortality of the most prevalent cancers among men and women in Algeria (2022) [165]	12
2.1	Comparison of the reviewed methods according to few criteria.	40
3.1	Summary of RicIU-Net model performance at epoch 60 for training and validation phases.	52
3.2	Comparison of performance metrics between RicIU-Net and existing methods. . . .	54

List of Abbreviations

- **MRI** : Magnetic Resonance Imaging
- **DCE-MRI** : Dynamic Contrast-Enhanced Magnetic Resonance Imaging
- **CAD** : Computer-Aided Diagnosis
- **CNN** : Convolutional Neural Network
- **U-Net** : U-Shaped Neural Network
- **RicIU-Net** : Rician-Injected U-Net
- **DSC** : Dice Similarity Coefficient
- **IoU** : Intersection over Union
- **GPU** : Graphics Processing Unit
- **BRCA** : Breast Cancer Gene
- **PET** : Positron Emission Tomography
- **CT** : Computed Tomography
- **TR** : Repetition Time
- **TE** : Echo Time
- **FA** : Flip Angle
- **ROI** : Region of Interest

General introduction

0.1 Scientific context

Breast cancer remains one of the most prevalent and life-threatening cancers among women worldwide [19]. Early and accurate detection of malignant lesions is essential to improve the prognosis and guide effective treatment strategies. In this regard, Dynamic Contrast-Enhanced Magnetic Resonance Imaging (DCE-MRI) is widely recognized for its ability to capture both morphological and functional information, making it a valuable tool in breast cancer diagnosis.

Furthermore, in the era of rapid technological advancement, Artificial Intelligence (AI) has become a powerful asset in healthcare. Among its many applications, a key one is the segmentation of breast tumors in DCE-MRI, which plays a crucial role in diagnosis, monitoring treatment, assessing therapeutic response, and planning surgical procedures. However, MRI data is often affected by noise, particularly Rician noise, which can significantly degrade image quality and hinder the performance of conventional segmentation models.

0.2 Addressed problematic

Manual interpretation of DCE-MRI images is time-consuming, prone to inter-observer variability, and often compromised by inherent MRI noise, especially Rician noise. To address these challenges, numerous computerized segmentation methods based on AI techniques, especially deep learning such as U-Net [149], have been proposed in the literature. These latter, have shown considerable potential. However, most of them are trained under ideal conditions, with limited exposure to noisy data, which compromises their robustness and reliability in real-world clinical applications.

Therefore, the core problem addressed in this work is the design of a segmentation approach that can withstand the degradation caused by Rician noise, while maintaining high segmentation accuracy. Injecting this noise artificially during training may encourage the model to learn more robust and discriminative representations, better suited to real-world acquisition conditions.

0.3 Aimed objectives and research methodology

The primary objective of this research is to design, implement, and validate an automatic segmentation approach for DCE-MRI breast tumors, built upon U-Net [149] architecture. The proposed model, called *Rician-Injected U-Net (RicIU-Net)*, introduces a controlled injection of synthetic Rician noise into the encoding stage of U-Net. Specifically within the 4th and 5th blocks of the U-Net architecture, in order to enhance its robustness against the perturbations frequently encountered in real medical images.

Briefly, through the proposed RicIU-Net approach, we aim to:

- Enhance the segmentation accuracy of the standard U-Net for breast tumor segmentation, even under Rician noise conditions.
- Reduce dependence on complex preprocessing pipelines or external denoising techniques.
- Introduce a novel data augmentation strategy specifically tailored to the characteristics of MRI data.

The experimental study that aimed to evaluate the segmentation performance of the proposed RicIU-Net in comparison to the standard U-Net and one of its existing recent variant (U-Net2.1D [11]) has yielded encouraging results in favor of the proposed RicIU-Net. And this, on the well-known benchmark dataset BreastDM [194]. Therefore, the objectives outlined above have been, to some extent, successfully achieved.

0.4 Organization of the manuscript

This manuscript is structured into three main chapters. Below, we provide an overview of the content of each chapter.

The first chapter presents a general overview of breast cancer, highlighting the importance of early and accurate diagnosis through medical imaging. It also introduces classical image segmentation methods as well as the main challenges encountered in the segmentation of breast tumors.

The second chapter is dedicated to a detailed review of the state of the art in breast tumor segmentation using DCE-MRI. It analyzes approaches based on deep learning, particularly Convolutional Neural Networks (CNNs) and their variants. This chapter identifies the limitations of existing methods and justifies the need for a novel approach.

The third chapter describes the main contribution of this work, namely: the RicIU-Net approach. This chapter details also the experimental phase to assess the exhibited approach, including training and validation phases, and performance evaluation using standard metrics such as the Dice coefficient (DSC) and Intersection over Union (IoU). A comparison with standard U-Net and

one of its most recent variants is reported in the chapter to demonstrate the robustness of the proposed approach.

Finally, the manuscript concludes with a general conclusion that summarizes our main contributions and results, discusses the limitations encountered, and outlines future perspectives for improving the proposed method.

Chapter 1

General overview of breast cancer and image segmentation

1.1 Introduction

Breast cancer remains one of the leading causes of mortality among women worldwide. Despite extensive research, its exact causes are not fully understood. Hence, early detection and timely intervention remain the most effective strategies for improving survival rates. In this regard, biomedical imaging has become an essential tool in modern medicine, providing advanced technologies for detailed visualization of internal structures. These imaging modalities offer crucial insights for diagnosing, characterizing, and monitoring breast tumors.

Among the available screening and diagnostic techniques, Magnetic Resonance Imaging (MRI) is widely recognized for its superior sensitivity. Unlike conventional methods, MRI provides high-resolution imaging of soft tissues, making it particularly effective in detecting tumors that other modalities might miss. However, accurate interpretation of MRI scans relies on sophisticated image processing techniques, particularly image segmentation, which is vital for delineating tumor boundaries and distinguishing cancerous from healthy tissues. Specifically, image segmentation is considered as a key computational technique in medical imaging that enhances the accuracy of tumor identification and extraction. Therefore, it improves diagnostic precision and allows healthcare professionals to assess tumor size, shape, and progression more reliably.

Given these considerations, this chapter provides an overview of breast tumors, including their characteristics, diagnosis, and treatment. It also explores the fundamental principles of image segmentation, with a special focus on deep learning-based techniques. The chapter is structured as follows: Section 3.2 provides an overview of breast anatomy and the classification of breast tumors. Section 3.3 introduces biomedical imaging and examines key imaging modalities used for the detection of breast cancer. Section 3.4 outlines the most commonly adopted treatment approaches. Finally, Section 3.5 delves into the principles of image segmentation and highlights various seg-

mentation techniques applied in medical imaging. The chapter concludes with a summary of key findings in Section 3.6.

1.2 Anatomy and epidemiology

In this section, we present the anatomy of the breast and breast tumors. Additionally, we classify these tumors and conclude by discussing relevant statistical data at both the global level and in Algeria.

1.2.1 Normal anatomy of the breast

The breast is a paired organ located in the anterior and upper part of the thorax. It contains the mammary gland, which is responsible for milk secretion [154], and plays a crucial role in femininity. Functionally, it serves both nutritional and aesthetic purposes. Although the breast is predominantly developed in women, it also exists in vestigial form in men.

From an anatomical perspective, the female breast is composed of glandular, fibrous, and adipose tissues. It is positioned above the pectoralis major muscle and is anchored to the thoracic wall by Cooper's ligaments [141], which provide structural support. The soft consistency and shape of the female breast is mainly attributed to the layer of adipose tissue. The fibrous connective tissues and glandular structures contain lobules, which are responsible for milk production. Figure 1.1 illustrates the anatomical structure of the female breast.

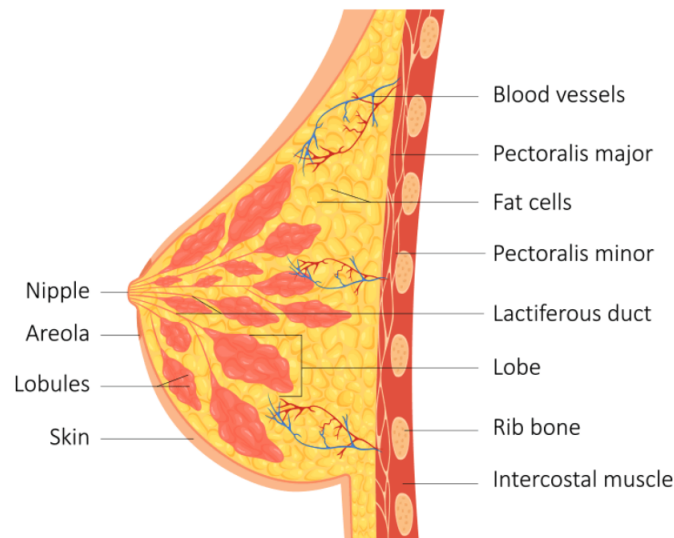


Figure 1.1: Illustration of a sagittal view of the anatomical structure of the female breast [174]

1.2.2 Breast tumor

A *tumor* is an abnormal growth of tissue caused by an abnormal cell proliferation. Tumors can be classified into two main categories: *benign* and *malignant*. Benign tumors are non-cancerous and generally do not spread to other parts of the body. In contrast, malignant tumors are characterized by uncontrolled growth and the potential to invade surrounding tissues or metastasize to distant organs, which defines them as cancerous.

On the other hand, breast tumors vary in nature depending on the type of tissue from which they originate. Some tumors result from benign breast conditions, such as fibrocystic changes, fibrosis, or localized lumps. These are usually not life-threatening and may not require aggressive treatment. However, some tumors are malignant (also called cancers) and typically develop in ductal cells (forming ductal carcinoma), lobular cells (leading to lobular carcinoma), or, in rarer cases, other breast structures. The majority of breast cancers originate in the milk ducts or lobules, as these areas are more susceptible to cellular abnormalities [73].

In addition, the onset of breast cancer is influenced by multiple factors, with genetic and hereditary predisposition playing a critical role. Individuals with a family history of breast cancer, particularly those with mutations in genes such as BRCA1 and BRCA2, are at significantly higher risk [119]. Beyond genetic factors, several environmental and lifestyle variables contribute to breast cancer incidence.

Also, key risk factors include hormonal, reproductive, and lifestyle influences. Early onset of menstruation (menarche) and late menopause increase a woman's lifetime exposure to estrogen, which has been linked to a higher risk of developing breast cancer. Similarly, reproductive factors such as having fewer children, late first pregnancy, and nulliparity (not having children) are associated with an increased risk. Exogenous hormone exposure, particularly through oral contraceptives and hormone replacement therapy (HRT), has also been implicated in some studies [21].

Furthermore, diet and body composition further contribute to risk. Research has shown that alcohol consumption and obesity, particularly weight gain in adulthood and increased visceral fat, can significantly elevate breast cancer risk. The role of nutrition, including the consumption of processed foods and high-fat diets, is also under investigation as a potential contributor [196].

On a positive note, certain protective factors have been identified. Breastfeeding is recognized for its protective effect, as it reduces lifetime exposure to estrogen and promotes cellular differentiation in breast tissue, thereby lowering cancer susceptibility. Additionally, regular physical activity has been linked to a lower risk of breast cancer by helping regulate hormone levels and maintaining a healthy body weight. These findings emphasize the importance of lifestyle choices in both cancer prevention and overall breast health [21].

Understanding these factors is crucial in developing effective breast cancer prevention strategies. While some risk factors, such as genetic predisposition, cannot be modified, lifestyle changes,

early screening, and advancements in medical research offer promising avenues for reducing breast cancer incidence and improving patient outcomes.

1.2.3 Classification of breast tumors

The classification of a tumor plays a crucial role in determining an accurate prognosis and developing an effective treatment plan. Among the various classification systems, the TNM (Tumor, Node, Metastasis) staging system is one of the most widely adopted for breast cancer. This system categorizes tumors based on three primary characteristics: the *size* of the tumor, the *extent of lymph node* involvement, and whether the *cancer has metastasized* to distant organs. Each of these factors contributes to defining the severity of the disease and guiding clinical decisions regarding treatment.

The size of the tumor (T) is a fundamental criterion in staging, as larger tumors are generally associated with a more aggressive disease progression. In addition to tumor size, the presence of cancer in lymph nodes (N) is another key factor. Lymph nodes serve as part of the body's immune defense, and when cancer spreads to these structures, the likelihood of further metastasis increases. The final criterion, metastasis (M), refers to whether cancer has spread beyond the breast and regional lymph nodes to other parts of the body, such as the liver, lungs, bones, or brain.

As the tumor progresses through these stages, the prognosis typically worsens. A small, localized tumor that has not spread beyond the breast has a much better prognosis than a tumor that has invaded multiple lymph nodes or metastasized to distant organs. The TNM classification system allows oncologists to determine the most appropriate therapeutic approach, which may include surgery, chemotherapy, radiation therapy, targeted therapy, or a combination of these treatments. By accurately staging the disease, clinicians can personalize treatment strategies and improve patient outcomes.

More details on the different stages of breast cancer tumors are illustrated in Figure 1.2.

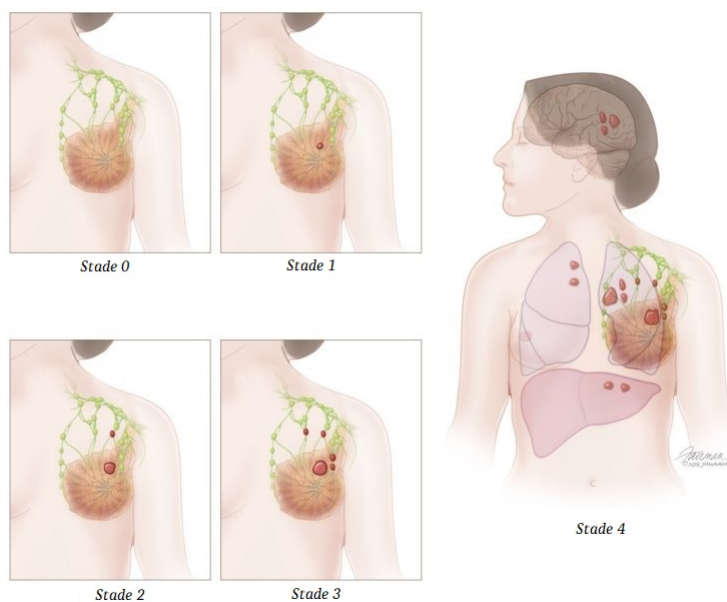


Figure 1.2: Illustration of breast tumor stages according to the TNM system [162]

1.2.4 Statistics on breast cancer

1.2.4.1 Worldwide statistics

According to Bray et al. [19], approximately 2.3 million cases of female breast cancer were diagnosed globally in 2022, making up nearly one in every four cancer cases among women. Consequently, breast cancer remains the most prevalent cancer among women and is the second most commonly diagnosed cancer overall. Figure 1.3 shows a pie chart representing the incidence rate of cancer worldwide in 2022, while Figure 1.4 illustrates the global mortality rate from cancer in the same year. Furthermore, the authors report that breast cancer is the most frequently diagnosed cancer in the majority of countries worldwide and continues to be the leading cause of cancer-related deaths in over 100 countries.

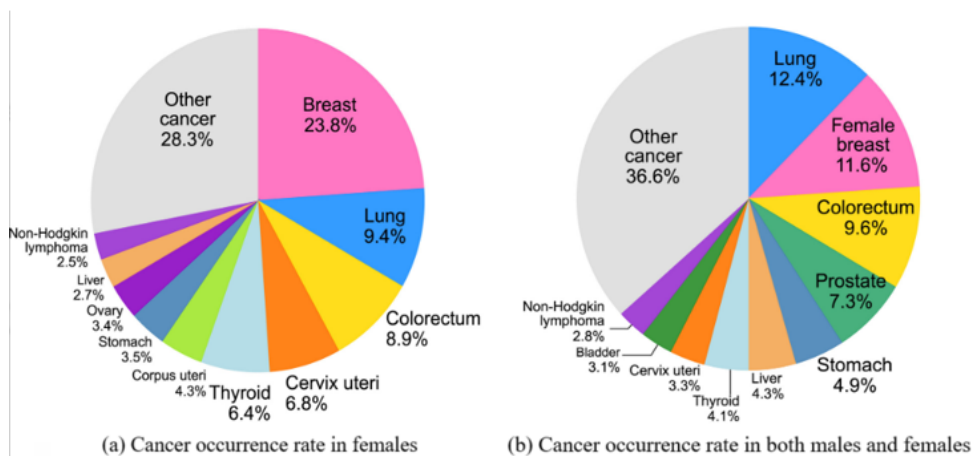


Figure 1.3: Pie chart of the global cancer incidence rate in 2022 [165]

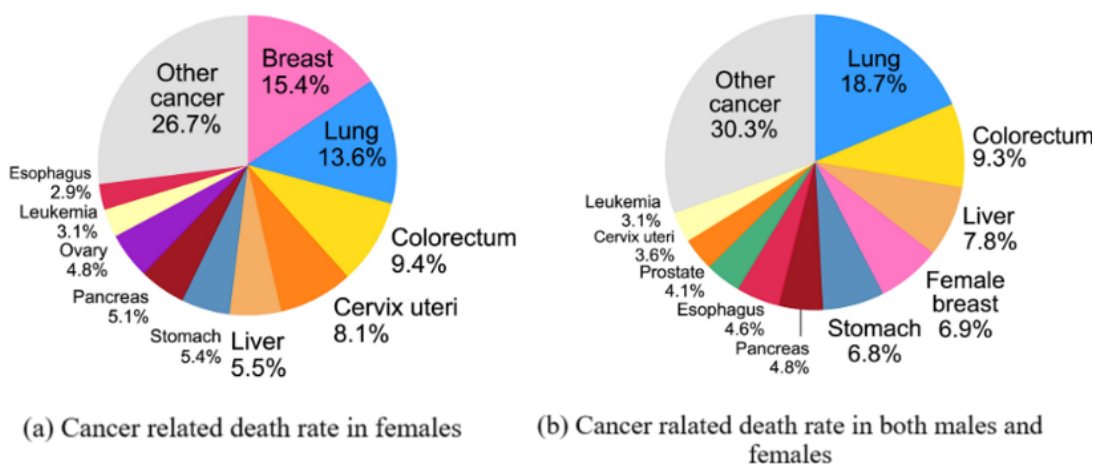


Figure 1.4: Pie chart of the global cancer incidence rate in 2022 [165]

Specifically, the incidence rate of breast cancer remains higher in developed countries such as Australia/New Zealand, European nations, and North America. In addition, over the past few decades, many transitioning countries in South America, Africa, and Asia have experienced a steady rise in the disease’s incidence [bray2]. However, breast cancer mortality shows less variability compared to incidence rates, with the highest mortality observed in Melanesia, where Fiji continues to report among the highest mortality rates globally. Figure 1.5 illustrates a bar chart that shows age-standardized incidence and mortality rates by region for female breast cancer in 2022.

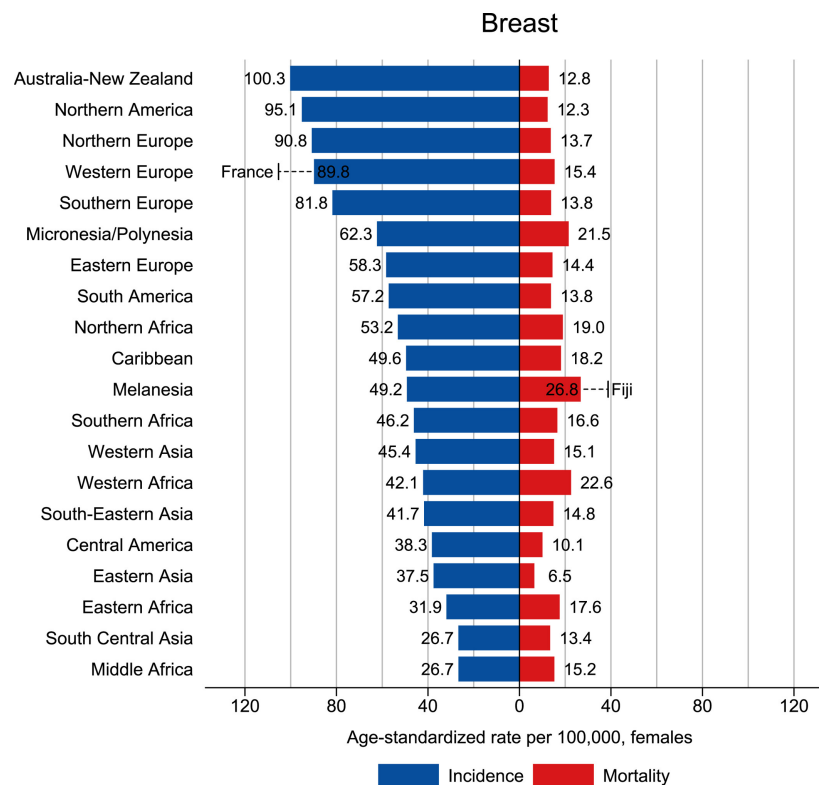


Figure 1.5: Bar chart of age-standardized incidence and mortality rates by region for female breast cancer in 2022 [165]

1.2.4.2 In Algeria

In Algeria, the latest statistics published in 2022 by the Global Cancer Observatory [60] of the World Health Organization [132] confirm that breast cancer remains the most frequently diagnosed malignancy, with 14,601 new cases reported in 2022, accounting for 22.6% of all cancer diagnoses. Furthermore, breast cancer constitutes a major public health concern as it represents the leading cause of cancer-related mortality among Algerian women, with 4,893 deaths recorded in the same year. Other prevalent cancer types include colorectal (7,747 cases), lung (5,040 cases), prostate (3,514 cases), and bladder (3,240 cases) cancers (see Table 1.1). These findings underscore the substantial burden of breast cancer in Algeria, positioning the country among the most affected in the African region.

1.3 Biomedical imaging for breast cancer screening

Biomedical imaging is a field of medicine that has witnessed significant advancements with the evolution of computing technologies. The terms “*biomedical imaging*” and “*imaging diagnosis*” refer to a generic, non-invasive process that allows for the observation of areas within the body that are not externally visible. This approach plays a crucial role in preventive health programs

Cancer	Incidence	Mortality
Breast	14 601	4893
Colorectum	7747	4380
Lung	5040	4599
Prostate	3514	1333
Bladder	3240	1818

Table 1.1: Incidence and mortality of the most prevalent cancers among men and women in Algeria (2022) [165]

and is widely regarded as the most effective method for the early detection of tumors. Moreover, the applicability and effectiveness of each imaging technique are heavily dependent on the specific characteristics of the organ being imaged. Therefore, selecting the most appropriate imaging technique prior to examining an organ is essential for accurate results [14].

The following subsections provide a brief overview of the primary imaging modalities used in radiology for breast imaging and the diagnosis of associated abnormalities, namely: *mammography*, ultrasonography, *Computed Tomography (CT)*, *Positron Emission Tomography (PET)*, and *Magnetic Resonance Imaging (MRI)*. These methods have become integral to the detection, diagnosis, and monitoring of breast cancer, offering valuable insights that aid in early diagnosis, treatment planning, and patient management. Each modality has its own strengths and limitations, and their combination often provides complementary information that enhances diagnostic accuracy.

1.3.1 Mammography

Mammography is a widely used mass screening modality that employs a non-invasive radiographic technique to capture the internal structures of the breast in an image [153]. Specifically, it involves exposing the breast to low-energy ionizing radiation (X-rays) at 30 kVp to produce images on planar radiographic films. Mammography is considered one of the gold standards in breast imaging due to its simplicity, speed, high specificity, and wide availability. Additionally, it has the ability to detect tumors that are not yet palpable, making it an effective tool for identifying abnormalities at the pre-clinical stage.

However, mammography has several limitations. Notably, the use of ionizing radiation over time could potentially contribute to the development of tumors [61]. Furthermore, the quality of the images produced is often inferior compared to other imaging modalities. Mammography also faces challenges in detecting abnormalities in women with dense breast tissue, where it may not provide accurate or sufficient results [80]. Despite these drawbacks, mammography remains a crucial tool for breast cancer screening, particularly when used in conjunction with other imaging techniques to enhance diagnostic accuracy.

1.3.2 Ultrasonography

Ultrasonography is also a non-invasive screening modality that uses sound waves to create a visualization of the breast. Specifically, it operates on the principles of echo emission and the transmission of ultrasonic waves (ranging from 2 to 20 MHz). Higher frequencies produce clearer images but penetrate less deeply into the patient. Ultrasound is particularly useful in diagnosing whether a nodule is solid or fluid-filled [10]. Additionally, it has the ability to detect tumors that may not be clearly identified through mammography, especially in cases involving dense breasts (rich in glandular tissue), such as in women under the age of forty.

However, due to the relatively low resolution of breast ultrasound images, false positive results may occur [96]. Therefore, ultrasound requires radiologists with proper training and specialized skills, including manual dexterity and keen observational ability [120]. Furthermore, the application of a coupling gel between the probe and the breast is necessary to eliminate air refraction effects, ensuring optimal image quality for accurate diagnosis. Despite these limitations, ultrasound remains a valuable complementary tool in breast cancer screening, especially when combined with mammography to improve diagnostic accuracy.

1.3.3 Computed Tomography (CT)

Similar to mammography, *Computed Tomography* (CT), also known as tomography by computer, uses ionizing radiation (X-rays). However, it allows for the production of tomographic slices (or planes) of the breast. As a result, CT provides a three-dimensional visualization of the organ [69]. Despite this capability, computed tomography offers limited advantages for breast cancer diagnosis, as it does not provide as much significant information compared to mammography. Furthermore, it complicates the acquisition process by increasing the dose of X-rays, which raises concerns about radiation exposure. Consequently, CT is rarely used as a primary modality for breast cancer screening but may be considered in certain clinical situations, such as when more detailed anatomical information is needed for staging or evaluating the extent of disease.

1.3.4 Positron Emission Tomography (PET)

Positron Emission Tomography (PET) is a nuclear medicine imaging modality in which a small amount of radioactive liquid material is injected into the body and used to diagnose various diseases, including breast tumors. Typically, in PET, a simple sugar is used as the radioactive substance, which is directly injected into the bloodstream. As a result, it accumulates in areas of the body where it releases energy in the form of gamma rays [32]. These gamma rays are detected by the PET scanner as signals, which are then converted by a computer into detailed images showing the functioning of tissues or organs.

More specifically, tumor cells require sugar for growth. Therefore, by monitoring how sugar is

utilized in the body (or sugar metabolism), the PET scanner is capable of detecting tumors. PET provides physiological information about the tumor being examined, in contrast to other imaging modalities that primarily capture morphological data. Furthermore, PET is often employed to diagnose or stage metastases or to search for contaminated lymph nodes [183]. This makes PET a valuable tool for assessing the metabolic activity of tumors and for detecting early-stage malignancies that may not be visible on other imaging modalities.

1.3.5 Magnetic Resonance Imaging (MRI)

According to Semchedine [155], *Magnetic Resonance Imaging (MRI)* is a highly effective and entirely non-invasive imaging modality. In brief, the principle of this biomedical imaging technique is based on the magnetization phenomenon of hydrogen protons when exposed to an electromagnetic field. The MRI scanner primarily consists of a powerful magnet that emits electromagnetic waves. These waves induce the magnetization of hydrogen protons present in the tissues of the examined organ. During this magnetization state, the protons absorb energy and align with the direction of the applied field.

Once the electromagnetic wave emission ceases, the protons gradually return to their initial state, releasing the absorbed energy in the form of a radio signal, known as *Free Induction Decay (FID)*. This signal is intercepted and measured by specialized receivers. The received signal is then processed by a computerized system to construct high-precision anatomical slices. These slices are subsequently assembled into a final MRI volume, providing detailed internal structural visualization of the targeted organ.

In 1971, Damadian [40] was the first to conceive the idea of a scanner using magnetic resonance to detect cancer in tissues. However, Lauterbur [93] was the first to utilize such a machine for diagnostic purposes, publishing the first clinical MRI image in 1973. A schematic representation of Damadian's machine is illustrated in Figure 1.6, while a depiction of a modern MRI scanner is shown in Figure 1.7.

1.3.5.1 MRI parameters and sequences

Various types of MRI sequences can be generated by modifying the sequencing parameters of the MRI system. To obtain the desired sequence, three essential parameters must be manually adjusted to their appropriate values using a dedicated control console. These parameters are as follows [155]:

- *Echo Time (ET)*: Refers to the time interval between the application of a radio frequency (RF) excitation pulse and the peak of the resulting FID signal.
- *Repetition Time (RT)*: Represents the time separating two successive RF excitations. It

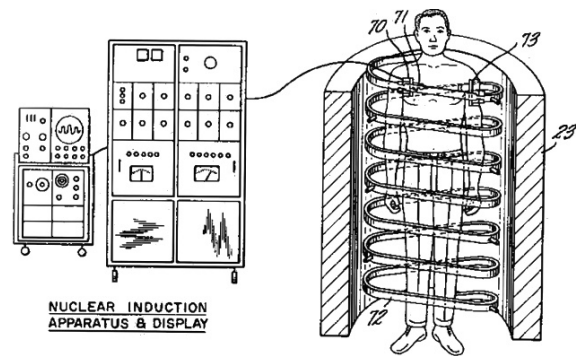


Figure 1.6: Schematic representation of Damadian's machine [39]



Figure 1.7: Representation of a modern MRI scanner [76]

determines the amount of magnetization recovered between each pulse. Both ET and TR are measured in milliseconds and are considered contrast factors.

- *Flip Angle (FA)*: This parameter controls the orientation of hydrogen protons in response to an RF excitation pulse.

Furthermore, the most commonly used MRI sequences for breast imaging are as follows [32, 155] :

- *Proton Density (PD)* : Obtained by using a short ET and a long RT.
- *T1-weighted (T1w)* : Achieved by using a long ET and a long RT. Useful for highlighting breast parenchyma or adipose tissue.
- *T2-weighted (T2w)* : Obtained using a short ET and a short RT. Effective for visualizing water-rich tissues such as cysts.

To obtain clearer images, a fat saturation technique is applied to suppress the signal from adipose tissue. This technique can be applied to both T1w and T2w sequences by utilizing the short relaxation times of adipose tissue [140]. When the fat signal is suppressed in a T1w image (or T2w), the resulting image is referred to as a fat-saturated T1-weighted image (or fat-saturated T2-weighted image).

1.4 Breast cancer treatment

After obtaining the results from medical imaging, the attending physician establishes a treatment plan based on the findings. The most commonly used treatments are surgery and therapy, but a combination of both can also be considered.

1.4.1 Lumpectomy

Lumpectomy is a breast-conserving surgical procedure in which the surgeon removes the tumor from the breast along with a surrounding margin of normal tissue (referred to as the “margin”). To perform this, the surgeon makes an incision ranging from two to seven centimeters on the breast and surgically removes the tumor along with a border of surrounding healthy breast tissue to ensure the complete removal of the affected area [171]. Post-lumpectomy, radiation therapy is required to eliminate any microscopic cancerous cells that may remain in the remaining breast tissue, thereby reducing the likelihood of local recurrence (reappearance of the same treated tumor).

1.4.2 Mastectomy

Non-conserving breast surgery, or *mastectomy*, involves the removal of all breast tissue from the chest wall [152]. Different types of mastectomy may be performed:

- *Total mastectomy*: The entire breast is removed, but the pectoral muscles beneath the breast tissue and the lymph nodes are preserved.
- *Modified radical mastectomy*: The entire breast is removed along with the affected axillary lymph nodes.
- *Skin-sparing mastectomy*: A total or modified radical mastectomy is performed, but most of the skin over the breast is preserved for reconstructive purposes.

It is important to note that mastectomy does not prevent cancer recurrence on the chest wall, and therefore, radiation therapy is recommended following the surgery [152]. Figure 1.8 illustrates the modified radical mastectomy.

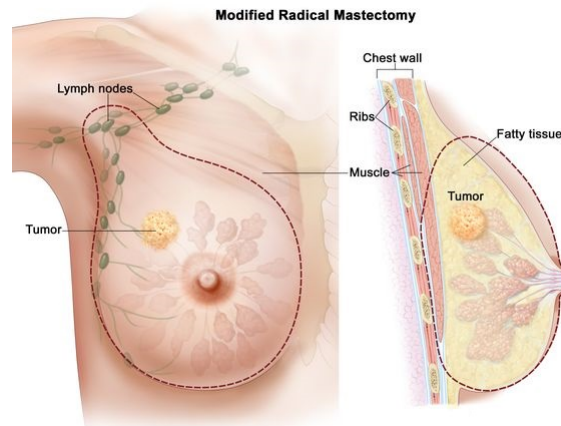


Figure 1.8: Illustration of the modified radical mastectomy [117]

1.4.3 Chemotherapy

Chemotherapy is a procedure that involves the use of anticancer drugs (or a combination of drugs) to eliminate cancer cells [152]. There are three main situations where chemotherapy may be used:

- *Before surgery (neoadjuvant therapy)*: In this case, chemotherapy is used either to slow the development of a tumor or to reduce the size of larger tumors before tumor resection.
- *After surgery (adjuvant treatment)*: Used to reduce the risk of cancer recurrence.
- *Metastasis*: To destroy cancer cells that may have spread to other organs in the body.

1.5 Image segmentation: principles and methods

In this section, we present the fundamental principles of image segmentation in image processing, along with an overview of a couple of well known deep learning based methods in the literature.

1.5.1 Image processing

Image processing is a fundamental discipline aimed at analyzing an image to extract meaningful information or provide a semantic interpretation of the objects it contains. It encompasses two primary types of processing: *low-level* and *high-level* processing.

Low-level processing algorithms focus on the relationships between the numerical values of image pixels without considering their real-world significance [83]. These operations typically include tasks such as noise reduction, contrast enhancement, and edge detection. In contrast, *high-level* processing algorithms analyze the information extracted by low-level techniques to symbolically

describe or interpret the content of the image [143]. This stage often involves object recognition, classification, and scene understanding.

The image processing workflow is generally structured into four key stages: *pre-processing*, *segmentation*, *feature analysis*, and *interpretation*. The first two stages (*i.e.* pre-processing and segmentation) are considered low-level processing tasks, as they primarily deal with pixel-level transformations and region extraction. The last two stages (*i.e.* feature analysis and interpretation) fall under high-level processing, as they aim to derive meaningful insights from the segmented image, enabling decision-making in various applications such as medical imaging, remote sensing, and autonomous vision systems.

1.5.1.1 Definition of image segmentation

The term *image segmentation* refers to the process of partitioning an image into groups of pixels, also referred to as regions or segments, that share uniform characteristics. This process highlights each homogeneous region in a manner that allows it to be easily distinguished from others [61]. The combination of the resulting regions reconstructs the entire image. Image segmentation is primarily used to detect Regions of Interest (ROIs) or to delineate the boundaries of regions within an image. For clarity, an illustration of an image and two possible corresponding segmented images are provided in Figure 1.11.

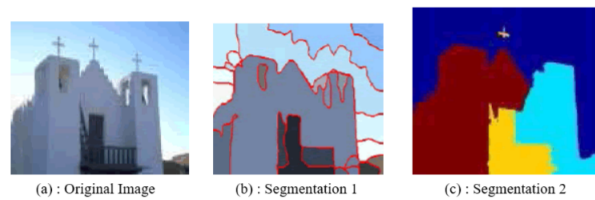


Figure 1.9: Illustration of an original image and its two possible segmented versions, demonstrating the image segmentation process [84]

1.5.1.2 Mathematical definition of image segmentation

A mathematical definition of image segmentation was proposed by Horowitz and Pavlidis [72]. Specifically, given an image Ω to be segmented, the segmentation process aims to partition the image into N sub-regions, denoted R_i , where $i = 1, 2, \dots, N$ and $L(\cdot)$ is a logical predicate that measures the homogeneity of a given region relative to a predefined set of features.

$$\Omega = \bigcup_{i=1}^N R_i, \quad (1.1)$$

$$R_i \cap R_j = \emptyset, \forall i, j \in \{1, 2, \dots, N\}, \quad (1.2)$$

$$L(R_i) = \text{True}, \forall i \in \{1, 2, \dots, N\}, \quad (1.3)$$

$$L(R_i \cup R_j) = \text{False}, \forall i, j \in \{1, 2, \dots, N\}, i \neq j. \quad (1.4)$$

The definition includes four key conditions: Condition (1.1) implies that every pixel in the image is assigned to one region of the image, covering the entire image domain. Condition (1.2) states that each pixel must be assigned to exactly one region, ensuring mutual exclusivity between regions. Condition (1.3) requires that the resulting regions are homogeneous with respect to some predefined feature set (such as color, intensity, texture, etc.), meaning that pixels within a region share similar characteristics. Condition (1.4) indicates that the union of two distinct regions, each homogeneous by itself, results in a heterogeneous region. This condition implies that regions can be merged if and only if their combination results in a non-homogeneous region, reinforcing the segmentation as a process of finding meaningful boundaries in the image. These conditions form the foundation of a rigorous approach to image segmentation, ensuring that the segmented regions are both distinct and homogeneous.

1.5.1.3 Over-segmentation vs Under-Segmentation

The number of segments is a crucial criterion in assessing the quality of an image segmentation. An imbalance in the number of segments, either too many or too few, can lead to undesirable results. *Over-segmentation* occurs when the number of segments produced exceeds the expected number of segments [173]. This situation arises, for example, when a ROI in an image is divided into multiple semantically insignificant segments, instead of being segmented into a single connected region. In this case, the resulting segments are often too small or lack semantic coherence, making them inadequate for meaningful analysis. Despite being an undesirable outcome, over-segmentation is frequently employed in various research contexts as a preliminary step to simplify the computational complexity of more resource-intensive methods. Specifically, an over-segmented image, compared to its raw form, can be used as input for complex techniques, where each segment is treated as a superpixel. These adjacent and similar segments are then merged to produce a more accurate and fine-grained segmentation.

On the other hand, *under-segmentation* refers to a segmentation that produces fewer segments than expected. This problem is generally more challenging to address than over-segmentation [25]. One common solution is to re-segment the under-segmented image; however, this approach may not always be suitable, particularly when the image contains overlapping segments. In such cases, the application of re-segmentation could exacerbate the issue, leading to over-segmentation. While both over-segmentation and under-segmentation are well-recognized phenomena in the literature,

there is no universally accepted method to resolve these issues. Nonetheless, over-segmentation is often preferred over under-segmentation because it serves as a useful preprocessing step before applying more refined segmentation techniques [14]. Over-segmentation generally provides a more detailed segmentation map, which can later be merged into more meaningful regions, improving the accuracy of the final segmentation.

1.5.1.4 Automatic and semi-automatic segmentation

Semi-automatic segmentation requires minimal user involvement in the segmentation process [18]. This type of segmentation is particularly useful when the user desires to control or guide the segmentation, such as specifying the ROI to be segmented or fine-tuning the precision of the obtained result [62]. The semi-automatic approach strikes a balance between automation and user control, allowing for customized intervention to improve accuracy or adjust parameters based on user expertise or specific needs.

In contrast, *automatic segmentation* aims to fully automate the process, utilizing advanced algorithms and prior knowledge to enable the computer to determine the final segmentation result without any human intervention. These methods rely heavily on machine learning, statistical models, or deep learning techniques to analyze image features and make segmentation decisions autonomously.

When comparing the two types of segmentation, semi-automatic methods are more widely presented in the literature, despite the growing interest in minimizing human involvement as much as possible in automatic segmentation methods [62]. The primary advantage of semi-automatic segmentation lies in its flexibility and adaptability, allowing users to intervene and refine results when necessary, while still benefiting from the efficiency of automation. However, automatic segmentation methods, driven by advancements in artificial intelligence and deep learning, are becoming increasingly capable of achieving high-quality results with minimal human oversight, making them an area of active research for a wide range of applications.

1.5.1.5 Objectives of image segmentation

Image segmentation is a low-level processing technique that serves as a fundamental and essential step in image analysis. Specifically, the goal of segmentation is to simplify the representation of an image into something more meaningful and easier to analyze [78]. By doing so, it reduces the complexity of subsequent high-level processing required to interpret the image. As a result, successful image segmentation often leads to more accurate and effective high-level results [145]. For instance, in pattern recognition, precise segmentation of a ROI enables the extraction of representative feature vectors such as size, shape, color, and location, which in turn facilitates the recognition process.

Due to its crucial role, image segmentation methods are widely applied across various fields,

including medical image processing, content-based image retrieval, remote sensing, and more. In medical imaging, for example, accurate segmentation of tissues and organs plays a pivotal role in diagnostic procedures, while in remote sensing, segmentation helps in identifying and classifying land cover types. The versatility and significance of segmentation make it a key area of research and application in computer vision.

1.5.2 Deep learning for image segmentation

Deep learning has revolutionized the field of medical image analysis, particularly in the segmentation of complex images. Traditional image processing techniques often fail to handle the variability and intricate details present in medical images. Deep learning models, by learning hierarchical representations directly from the data, provide more precise and automated segmentation. This advancement has a profound impact on clinical applications such as tumor detection, diagnosis, and treatment planning [94]. In what follows, we briefly describe four widely used deep learning methods for medical image segmentation in the literature.

1.5.2.1 Convolutional Neural Networks (CNNs)

Convolutional Neural Networks (CNNs) are a class of deep feed-forward architectures that automatically learn hierarchical, spatially localized feature representations directly from raw images [94]. By stacking convolutional layers with nonlinear activations and pooling operations, CNNs capture increasingly abstract patterns, ranging from simple edges to complex textures. Thus, making them highly effective for visual tasks, including medical image segmentation.

- **Convolutional layers:** These layers apply a set of learnable filters to the input image. Each filter performs a convolution operation, producing feature maps that capture essential local patterns such as edges, textures, and shapes. This operation is critical for extracting spatial hierarchies within the image [88].
- **Activation functions:** Non-linear activation functions (e.g. ReLU) are applied after convolutional operations to introduce non-linearity into the network. This step is essential for enabling the network to learn complex representations of the input data [94].
- **Pooling layers:** Pooling layers, such as max pooling, reduce the spatial dimensions of the feature maps. This reduction not only lowers the computational cost but also provides a degree of translation invariance, making the model more robust to variations in input images.
- **Fully connected layers:** In many classification tasks, fully connected layers are used to integrate features and make final predictions. However, in segmentation networks like U-Net, an encoder-decoder structure is employed to preserve spatial information, replacing the traditional fully connected layers [149].

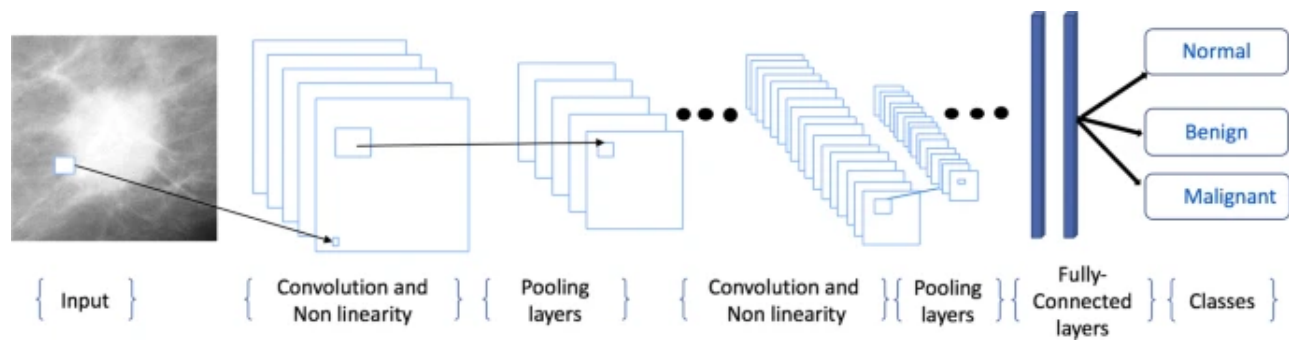


Figure 1.10: Example of a CNN architecture designed for tumor classification [1].

In medical imaging, segmentation is vital for accurately delineating ROIs, such as tumor boundaries in modalities like MRI, CT, and mammography. Accurate segmentation enables the extraction of critical information such as tumor size, shape, and location, which is essential for diagnosis and treatment planning. Advanced CNN architectures, including Fully Convolutional Networks (FCN) [110] and U-Net [149], have been specifically designed to meet the challenges of medical image segmentation. Comprehensive surveys have demonstrated that these deep learning models not only automate the segmentation process but also achieve performance levels comparable to human experts [104].

1.5.2.2 U-Net

U-Net is a fully convolutional neural network originally designed for biomedical image segmentation. Its strength lies in its ability to learn from very few training images while producing precise pixel-wise segmentation maps. The U-Net architecture consists of two main parts:

- **Encoder (contracting path):** This part is similar to a standard convolutional network. It applies a series of convolutional layers (typically with 3×3 kernels) followed by non-linear activations and max pooling operations. As the spatial dimensions decrease, the number of feature channels increases, enabling the network to capture the global context.
- **Decoder (expansive path):** The decoder upsamples the feature maps using up-convolution (or transposed convolution) to restore the original spatial resolution. At each upsampling step, features from the corresponding encoder layer are concatenated via skip connections, which help in recovering fine-grained spatial details.

The **skip connections** directly link corresponding layers in the encoder and decoder, fusing low-level spatial details with high-level semantic information. This U-shaped design allows the network to produce precise segmentation boundaries even when trained with limited data [149]. Figure 1.11 presents the architecture of the U-Net model.

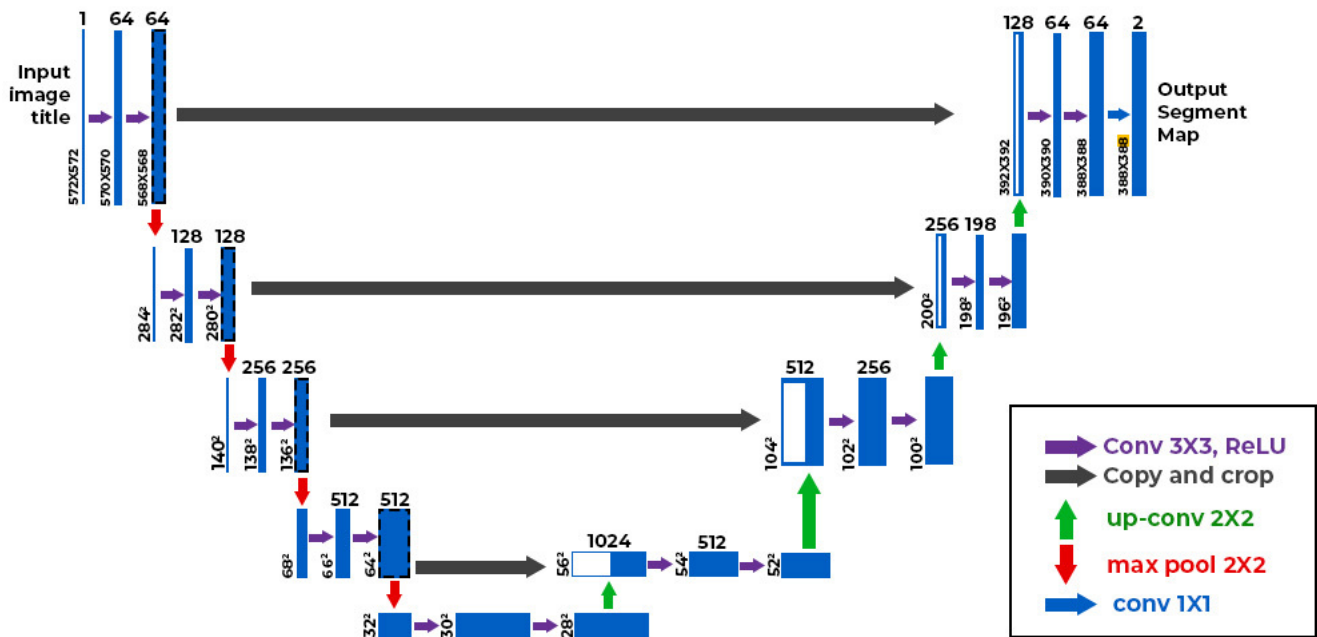


Figure 1.11: U-Net architecture (example for 32x32 pixels in the lowest resolution) [149]

1.5.2.3 Vision Transformer (ViT)

Vision Transformers (ViT) are a class of deep learning models that adapt the Transformer architecture, that is originally designed for natural language processing, to computer vision tasks, including image segmentation [44]. Unlike Convolutional Neural Networks (CNNs), which rely on local convolutional operations to extract spatial features, ViTs leverage self-attention mechanisms to capture global relationships across an entire image, offering a fundamentally different approach to processing visual data.

The ViT architecture begins by dividing an input image into a grid of fixed-size patches (e.g. 16x16 pixels). Each patch is flattened into a vector and linearly embedded into a higher-dimensional space, augmented with positional encodings to retain spatial information. These patch embeddings are then fed into a series of Transformer encoder layers. Each layer consists of two main components: a *multi-head self-attention* mechanism, which computes dependencies between all patches regardless of their spatial distance, and a *feed-forward neural network*, applied independently to each patch. Layer normalization and residual connections are used to stabilize training and improve gradient flow [170]. For segmentation tasks, ViT can be extended with a decoder, such as in models like SegFormer or TransUNet, to produce pixel-level predictions [176]. An example of the ViT's architecture is given in Figure 1.12 for visual illustration.

ViTs offer several advantages over CNNs, particularly for medical imaging applications like breast tumor segmentation. Their ability to model long-range dependencies makes them adept at capturing the global context of an image, such as the relationship between a tumor and surrounding

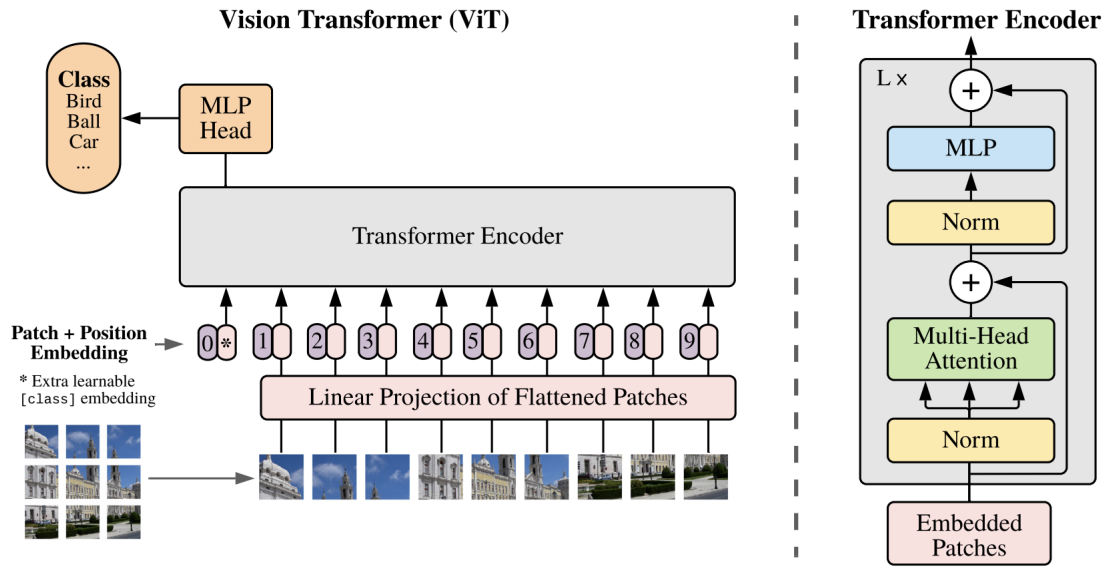


Figure 1.12: The Vision Transformer (ViT) architecture, where an input image is split into patches, embedded, and processed through Transformer encoder layers for classification or segmentation [44]

tissues in MRI scans, which may span beyond local convolutional receptive fields. Additionally, ViTs are highly flexible and can handle variable input resolutions when paired with appropriate positional encodings. However, they require large amounts of training data to outperform CNNs, as they lack the inductive biases (e.g. locality and translation invariance) inherent in convolutional operations. To mitigate this, pre-training on large datasets followed by fine-tuning on smaller medical datasets has become a common strategy [44].

In the context of breast cancer segmentation, ViTs have shown promise in recent studies. For instance, hybrid models combining ViTs with CNNs, such as TransUNet, leverage the strengths of both architectures: CNNs extract detailed local features, while Transformers model global interactions, improving tumor boundary delineation in complex MRI images [27]. While ViTs are computationally intensive due to their quadratic complexity with respect to the number of patches, advances like efficient attention mechanisms (e.g. Swin Transformer) are making them more practical for real-world applications [106]. This project could explore ViTs as an alternative or complement to U-Net, potentially enhancing segmentation accuracy by capturing both local and global tumor characteristics.

1.5.2.4 TransUNet

TransUNet is a hybrid deep learning architecture that integrates the strengths of Convolutional Neural Networks (CNNs) and Vision Transformers (ViTs) to enhance medical image segmentation, particularly for tasks like breast tumor delineation in MRI scans [28]. Originally proposed for 2D medical image segmentation, TransUNet combines the local feature extraction capabilities of U-Net with the global context modeling of Transformers, addressing the limitations of each approach when used independently.

The TransUNet architecture consists of three main components: an encoder, a bottleneck, and a decoder. The encoder employs a pre-trained CNN backbone (e.g. ResNet or EfficientNet) to extract low-level and mid-level features from the input image, capturing detailed spatial information such as edges and textures. These features are then transformed into a sequence of patch embeddings, similar to ViT, and processed through Transformer layers to capture long-range dependencies and global contextual information across the image. The bottleneck stage integrates these global features with local CNN features, enabling a richer representation of the image. Finally, the decoder, inspired by U-Net’s architecture, upsamples the feature maps using convolutional layers and skip connections to reconstruct high-resolution segmentation masks, preserving fine-grained details like tumor boundaries [28] (see Figure 2.1 for illustration).

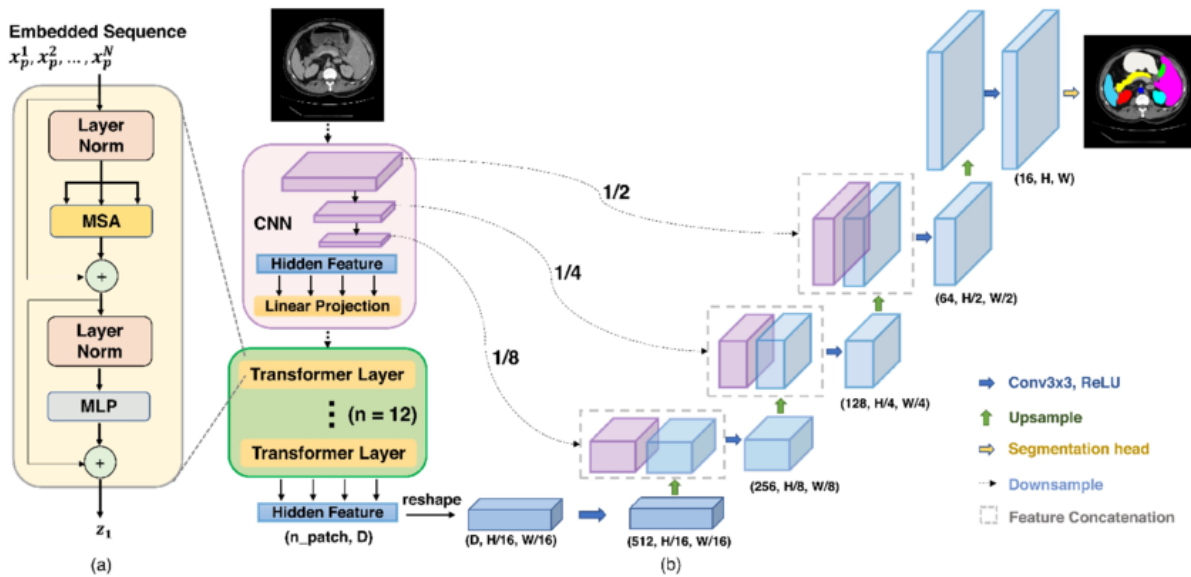


Figure 1.13: The TransUNet architecture, combining a CNN encoder, Transformer bottleneck, and U-Net-style decoder for medical image segmentation [27]

TransUNet offers significant advantages for breast tumor segmentation. Its CNN backbone excels at detecting local features, such as tumor edges and textures in MRI images, while the Transformer component models global relationships, such as the tumor’s interaction with surrounding tissues or its overall shape. This hybrid approach mitigates the data inefficiency of pure ViTs,

which require large datasets for training, and the limited receptive field of pure CNNs, which may miss global context. Studies have shown that TransUNet achieves state-of-the-art performance on medical segmentation benchmarks, including the Synapse dataset and breast cancer datasets, with improved Dice Similarity Coefficient (DSC) scores for tumor delineation [27].

In the context of this project, TransUNet is particularly promising for segmenting breast tumors in MRI scans. Its ability to combine local and global features could enhance the accuracy of tumor boundary detection, addressing challenges like irregular tumor shapes or low-contrast regions. However, TransUNet's computational complexity and memory requirements, due to Transformer layers, may necessitate efficient implementations or smaller models for real-time clinical applications. This project could explore TransUNet as a potential method, comparing its performance to U-Net or ViT on a breast cancer MRI dataset, potentially improving segmentation accuracy for clinical diagnosis and treatment planning.

1.6 Conclusion

The objective of this chapter was to provide an overview of breast cancer and image segmentation, serving as an introductory chapter to the broader topic. First, we defined breast cancer, biomedical imaging, and the existing treatment approaches used to combat this disease. We then introduced the fundamental principles of image segmentation and discussed some of the commonly used deep learning methods found in the literature.

In the next chapter, we will present a state-of-the-art review of various segmentation methods presented in the context of breast tumors DCE-MRI images, including 2D, pseudo 3D, and 3D approaches.

Chapter 2

State-of-the-art on DCE-MRI breast tumor segmentation

2.1 Introduction

Dynamic Contrast-Enhanced Magnetic Resonance Imaging (DCE-MRI) is a leading modality for breast cancer screening, providing detailed anatomical information alongside dynamic functional insight. However, its interpretation remains a complex and error-prone process when performed manually. Fortunately, image segmentation, a fundamental technique in computer vision, offers a promising solution by directing attention toward clinically relevant regions, such as tumors. Thereby enabling more efficient, accurate, and automated diagnosis.

In recent years, medical image segmentation has experienced significant advancements, largely driven by the rapid progress in deep learning technologies. As a result, various deep learning-based approaches have been proposed to automatically delineate breast tumor boundaries in DCE-MRI images. To offer a comprehensive understanding of these recent developments, this chapter provides a critical review and analysis of the most prominent state-of-the-art segmentation methods proposed within this scientific domain. The chapter is organized as follows: Section 3.2 presents the specifications related to the use of DCE-MRI in breast cancer screening and introduces the research problem addressed in this work. Section 3.3 provides a concise overview of recent deep learning-based approaches for breast tumor segmentation in DCE-MRI, as reported in the literature. Section 3.4 offers a comparative analysis of the reviewed methods, focusing on key aspects such as network architecture, dataset characteristics, and segmentation performance. Section 3.5 summarizes the findings, discusses current challenges, and outlines potential future research directions. Finally, Section 3.6 concludes the chapter.

2.2 Breast DCE-MRI and tumor segmentation

Dynamic Contrast-Enhanced MRI (DCE-MRI) for breast screening evolved from the broader development of MRI in medical imaging. The journey of DCE-MRI's development began with the discovery of Nuclear Magnetic Resonance (NMR) by Felix Bloch and Edward Purcell in 1946 [13]. Thereafter, Raymond Damadian proposed to use NMR for cancer detection in 1971, suggesting that malignant tissues exhibit distinct relaxation properties [41]. This assumption led to the creation of the first clinical MRI scanner a couple of years later [93, 114]. For breast imaging, it is in the 1990s that MRI gained prominence as a complementary tool for high-risk screening. Particularly after the introduction of DCE-MRI. Specifically, the latter involves injecting a gadolinium-based contrast agent to enhanced the visibility of regions of interest in the resulted DCE-MRI images, such as tumors.

Nowadays, DCE-MRI is extensively used to screen the breasts for tumor analysis for its remarkable high sensitivity, especially when the patient presents dense breasts or a high-risk of tumor. Specifically, DCE-MRI provides exhaustively detailed view of tumor morphology, vascularity, and kinetic patterns. In addition to this, it provides 3D high-resolution visualizations of the both breasts. Such important features, and several others, are not present in mammography or ultrasonography which are conventionally used in clinical routines. [89]. Figure 2.1 presents an illustration of the MRI scanner used to scan the breasts.

2.2.1 Analysis of DCE-MRI images to diagnose breast tumors

The *double reading* procedure is the methodology used in the traditional routine to analyze DCE-MRI breast images. Explicitly, two radiologists are charged to individually visualize the medical image to analyze and to write his/her interpretations of the findings in a report. If there are disagreements on interpretation, the two involved radiologists can either have a discussion about their opinions or seek advice from a third expert. However, like any human being, radiologists can face errors due to factors such as exhaustion, inattention, or even imperfections in the analyzed image due for instance to patient movement during the DCE-MRI exam. Consequently, the double reading procedure is not fully immunized. In this context, Nodine and Kundel [130] describe three main errors that can occur:

- A *visual error* that occurs when the presence of a tumor is not noticed. Usually because of a selective reading to focus on parts of the image that thought to be more interesting to explore.
- A *recognition error* that happens when a tumor is actually noticed, yet misidentified.
- A *decision-making error* that occurs when a tumor is identified, but misclassified.

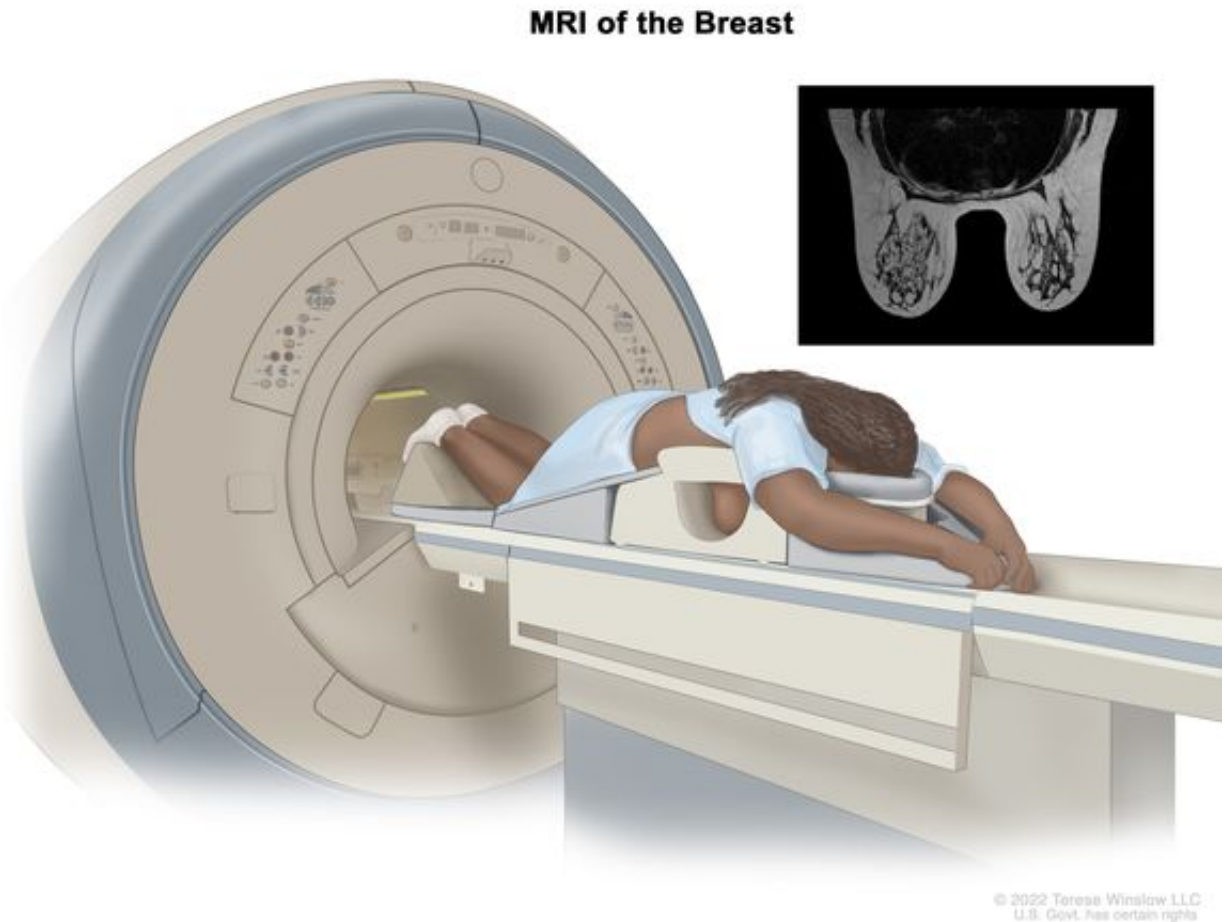


Figure 2.1: Illustration of a breast DCE-MRI scanner for cancer diagnosis [188]

Besides the possibility of error, DCE-MRI also imposes another challenge. Actually, the search area is large because the modality creates 3D scans with hundreds of slices to explore in the axial, sagittal, and coronal planes. Making the exploration process totally exhausting and time-consuming.

On the other hand, the integration of computer science, and more precisely artificial intelligence, in modern radiology has had a significant impact on dealing with these hurdles [122]. Specifically, artificial intelligence proposes a variety of computer methods that aid in the analysis of medical images to establish more reliable diagnoses, such as *Computer-Aided Diagnosis* (CAD) system. Specifically, a CAD system is a computer software that is specially conceived to help determine the type, severity, stage, progression, or regression of a tumor [33]. The *US Food and Drug Administration* approved the use of this system in 1998, since then it has been widely used as a second reader to interpret medical images [109]. Moreover, the advantages of such a system in diagnosing breast tumors in DCE-MRI, especially in dense breasts, have been demonstrated in several studies [57, 109, 185, 98]. Technically, a CAD system is made up of four main steps that

are carried out sequentially, namely: the *preprocessing* step, the *segmentation* step, the *features extraction and selection* step, and the *classification* step.

2.2.2 Importance of DCE-MRI breast tumor segmentation

Segmentation, as described in the previous chapter, is the process of distinguishing regions of particular interest from other regions in an image. Hence, in the case where the delimited regions are tumors, segmentation allows not only to delicately define the boundaries of the contaminated areas, but also offers a possibility to inspect their appearances [128]. Therefore, segmentation represents a critical step in a breast DCE-MRI CAD system since its result significantly affects the performance of the next steps. Specifically, the more accurate the tumor segmentation, the more discriminatory features can be extracted, hence the more realistic the prognosis can be [71].

Moreover, DCE-MRI breast tumor segmentation used as a standalone process, outside the CAD system framework, offers several benefits targeting two important healthcare aspects, namely: enhancing patient outcomes and maintaining breast esthetics. For patient outcomes improvement, segmentation identifies contaminated zones at their earliest stages (when they are likely not visible visually), and/or maps their size, shape, and location. As a result, it decreases unnecessary biopsies and prevents the development of aggressive breast cancers by enabling oncologists to customize timely treatment plans and to monitor the tumor. Particularly when there is a suspected return after ablation or to follow up changes in growth or response to treatment.

On the other hand, the esthetic aspect of DCE-MRI breast tumor segmentation resides is how it can improve surgical precision while maintaining the natural appearance of the breast. Explicitly, the use of segmentation to accurately identify tumor boundaries allows to remove only affected tissue of the breast. Which helps surgical teams avoid unnecessary excision to reduce breast asymmetry and hence the need for extensive reconstruction. In addition, it enables less invasive procedures, resulting in smaller scars and improved cosmetic results.

2.2.3 Challenge of breast DCE-MRI images segmentation for accurate extraction of tumors

Considerable efforts have been made to present the most effective method for optimal DCE-MRI breast tumor segmentation so far. Yet, even with many proposed approaches and registered appreciable performance scores in the literature, there is no clearly described final solution. Mostly, this is due to many facts and challenges that are acting as roadblocks in the development of a final algorithm. Bellow, we describe this challenges according to the different cases: *benign tumors*, *malignant tumors*, and *normal (healthy) breast tissue*.

- **Benign tumors:** Such as fibroadenomas or cysts. They typically appear as well-defined, smooth-edged masses on DCE-MRI. They often show slow, gradual, or no significant en-

hancement in the early phases, with minimal or no washout in late phases, reflecting low vascularity and stable perfusion [74]. These tumors pose segmentation challenges due to their similarity to normal tissue in contrast, requiring algorithms to distinguish subtle enhancement patterns without over-segmenting healthy areas (*i.e.* false positives). Figure 2.2 presents an example of a benign tumor of BreastDM dataset [194] showcasing an overlapping contrast with its surrounding uncontaminated tissue of the breast.

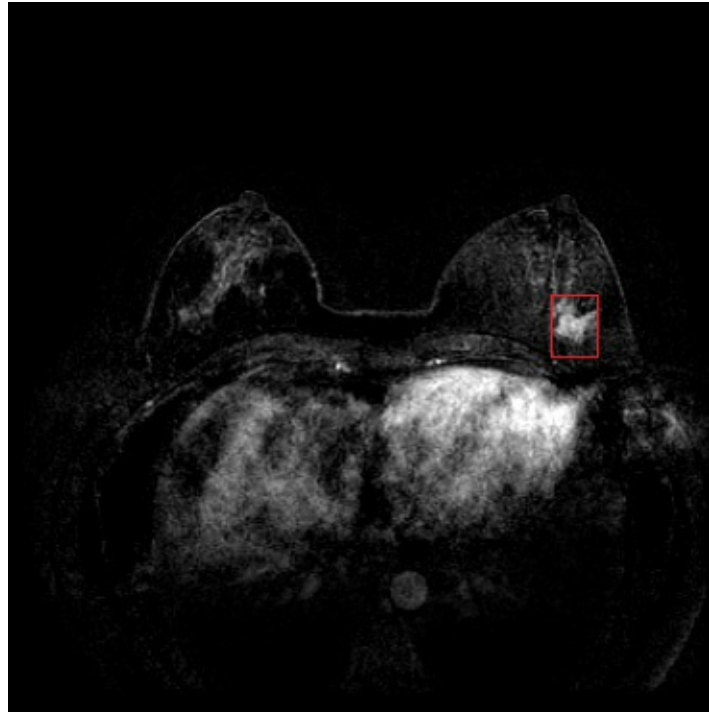


Figure 2.2: An illustration of a benign breast tumor highlighted with a bounded box in DCE-MRI taken from BreastDM dataset [194]

- **Malignant tumors:** Such as invasive ductal carcinoma or invasive lobular carcinoma. They exhibit rapid and irregular enhancement in the early DCE-MRI phases due to increased angiogenesis and vascular permeability, followed by a rapid washout in later phases [89]. These tumors often have irregular, spiculated margins and heterogeneous enhancement. Making them distinct from benign lesions but challenging to segment accurately due to their complex shapes and low-contrast boundaries with surrounding tissue. Automated segmentation must account for these dynamic patterns to avoid under-segmentation (*i.e.* false negatives). For visual illustration, we give in Figure 2.3 a malignant tumor seen in a DCE-MRI image taken from BreastDM dataset [194] presenting a complex shape and low contrast boundaries.

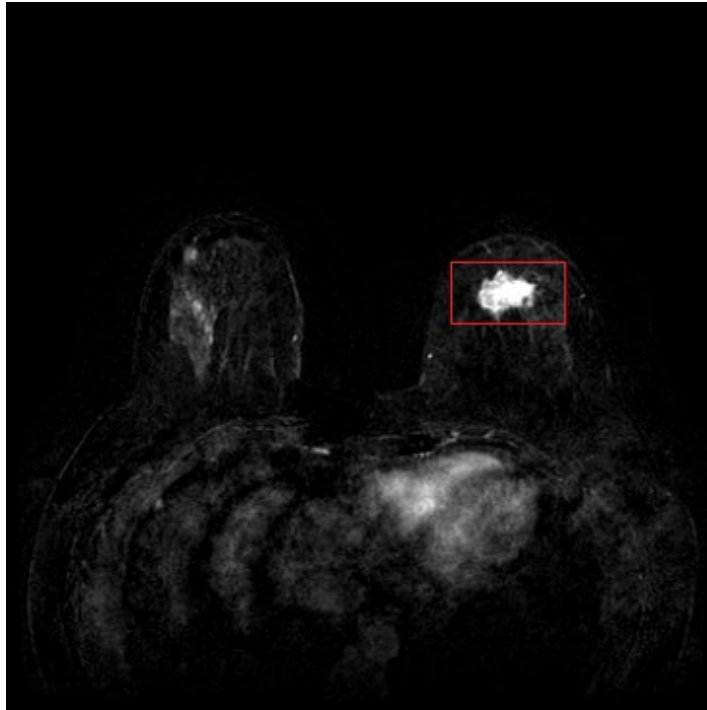


Figure 2.3: An illustration of a benign breast tumor highlighted with a bounded box in DCE-MRI taken from BreastDM dataset [breastdm2023]

- **Normal (healthy) breast tissue:** It includes glandular and fatty components and usually shows minimal or no enhancement in DCE-MRI, with uniform, low-level signal intensity across phases [102]. However, physiological enhancement in healthy breasts, such as background parenchymal enhancement or veins enhancements, with their variability can imitate tumor signals. These latter require robust algorithms to avoid misclassifying healthy regions as tumors. Figure 2.4 shows enhanced healthy regions of the breast in a DCE-MRI image.

These latter exhibited cases present distinct challenges for segmentation methods. Especially for deep learning based models, such as U-Net, Vision Transformers, and TransUNet, that have to be trained on well-confined datasets to master as many cases as possible. Furthermore, other challenges like overlapping enhancement, motion artifacts, variations in acquisition process, and the size of tumors can badly affect segmentation methods [102].

2.3 Description of related work

Since the apparition of the first deep learning based models, several research projects have reported their successful application to medical image analysis. Furthermore, their exceptional performance compared to traditional handcrafting methods has driven computer vision scientists to continuously improve them in order to accomplish challenging tasks like tumor extraction from medical

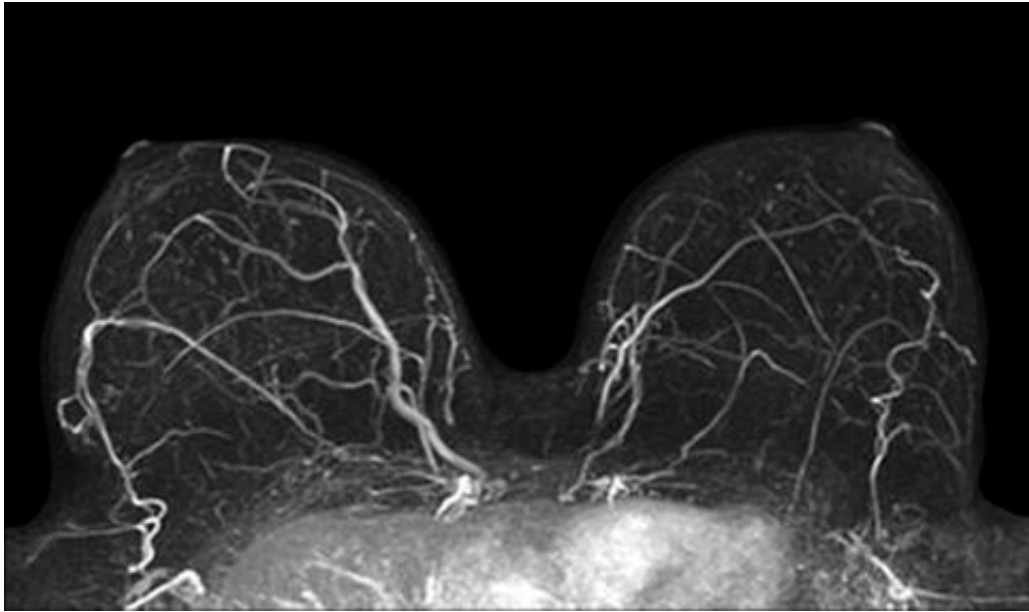


Figure 2.4: Illustration of a DCE-MRI image presenting different enhanced normal regions

images. Hence, giving rise to a very specific fine-tuned deep learning-based approaches adapted to a particular task, dataset, or domain. DCE-MRI breast tumor segmentation is no exception to the fact, given the number of deep learning-based approaches proposed in its context over the past decade. As a main goal to stand out and discuss the essential progress made recently by researchers in the framework, we aim to review and succinctly discuss, in this section, some of the latest and relevant state-of-the-art methods presented in the setting. The analyzed approaches are classified herein into *multiparametric* and *uniparametric data-driven methods*, based on the type of DCE-MRI data used for tumor feature extraction.

2.3.1 Multiparametric data-driven DCE-MRI breast tumor segmentation methods

These methods integrate multiple DCE-MRI sequences to extract comprehensive tumor features. Specifically, multiparametric data-driven approaches aim to enhance tumor representation by incorporating complementary information that may be missed when relying on a single sequence. However, these approaches require large datasets due to their dependence on multiple sequences. Building these datasets is challenging because of the complexity of the annotation and the limited availability of complete data in real-world clinical settings. Moreover, such methods present challenges when it comes to data heterogeneity and integration, as the sequences frequently differ in resolution, contrast, and noise characteristics. Furthermore, they are prone to overfitting and have a tendency to take too long to train, which can hinder their practical deployment. For instance, Peng et al. [139] have introduced an Inter-Modality Information Interaction Network

(IMIIN), an advanced deep learning model designed to provide a 3D multi-modal breast tumor segmentation in MRI imaging. IMIIN employs a hierarchical two-stage approach that begins with a coarse tumor localization phase, followed by a fine-grained segmentation stage utilizing a 3D Tiny Object Segmentation Network (3D-TOSN). This hierarchical design effectively captures detailed boundary information, making it particularly adept at segmenting small or complex tumors that are often challenging for traditional models. A central innovation in IMIIN is its Bi-directional Request-Supply Information Interaction Module (BD-RSIIM), which facilitates a dynamic, mutual exchange of information between T1 and T1c MRI sequences. This bi-directional interaction allows each modality to selectively request and incorporate relevant information from the other, filtering out irrelevant data and thereby improving the accuracy and robustness of tumor boundary segmentation. While IMIIN demonstrates notable improvements over existing models, such as 2D-CMN and HDN, achieving superior sensitivity and Dice similarity scores, the model's dependence on well-aligned multi-modal data could limit its applicability in diverse clinical settings where imaging data may not be perfectly aligned. Additionally, the model's complex architecture and high computational requirements could pose challenges in resource-limited environments. To address these limitations, future enhancements could incorporate a pre-alignment module to handle unaligned data, broadening the model's utility across varied clinical workflows. Furthermore, exploring lightweight architectural designs could reduce computational demands, making IMIIN more feasible for deployment in settings with constrained resources. These refinements would enhance the model's versatility and make it more adaptable and practical for widespread clinical application in breast cancer diagnosis. Figure 2.5 presents the architecture of the IMIIN network as it is exhibited by Peng et al. [139].

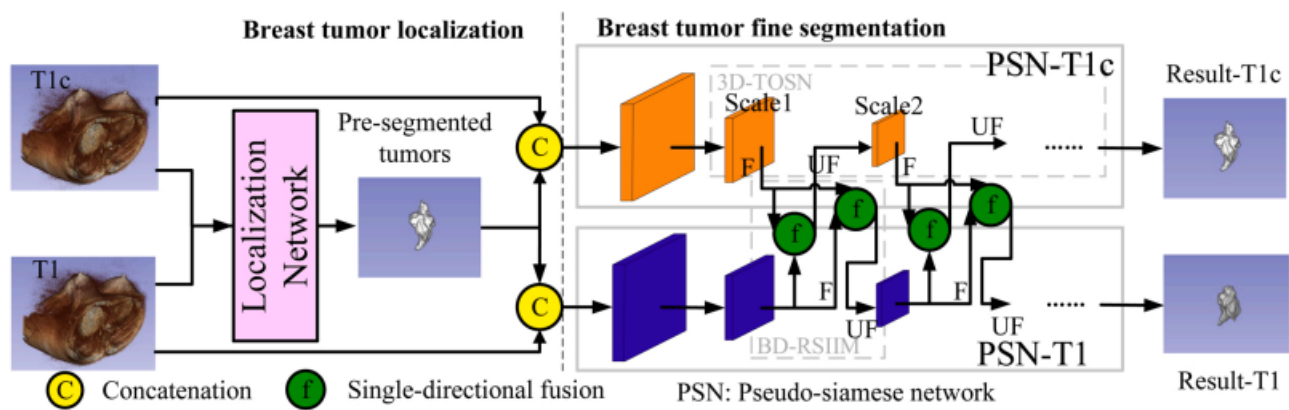


Figure 2.5: Illustration of the IMIIN network [139]

Furthermore, Liu et al. [105] have presented a mask-guided 3D convolutional neural network (3D-CNN) that analysis both pre-contrast and post-contrast DCE-MRI sequences to predict breast cancer outcomes. Specifically focusing on five-year recurrence and HER2 status, by analyzing DCE-MRI images. The model introduces a mask-guided 3D-CNN architecture to direct the

network's attention specifically to tumor regions, a method that enhances prediction accuracy over traditional models that either examine the entire image or focus solely on the tumor area. Techniques integral to this approach include dynamic contrast-enhanced MRI, which captures essential tumor characteristics, and class activation mapping (CAM), which visually highlights the regions that drive predictions, offering interpretability and precision. The model is built upon a modified 3D-VGGNet architecture optimized for volumetric data (see Figure 2.6 for illustration) and uses a loss function that combines cross-entropy with the Dice coefficient, promoting overlap between the model's attention and the tumor mask. To counter the small dataset (115 samples), 3D data augmentation techniques, such as rotations and translations, were employed, strengthening model robustness and reducing overfitting.

Despite promising results, there are limitations. Conservative segmentation might exclude relevant tumor areas, and the small dataset may limit generalizability. Future work could enhance this model by refining segmentation algorithms to include more of the tumor area, expanding the dataset, and comparing this mask-guided approach with traditional radiomics-based methods for further validation. This mask-guided 3D-CNN approach shows potential for improving the precision of prognostic predictions in clinical breast cancer applications, though further refinement and validation are essential.

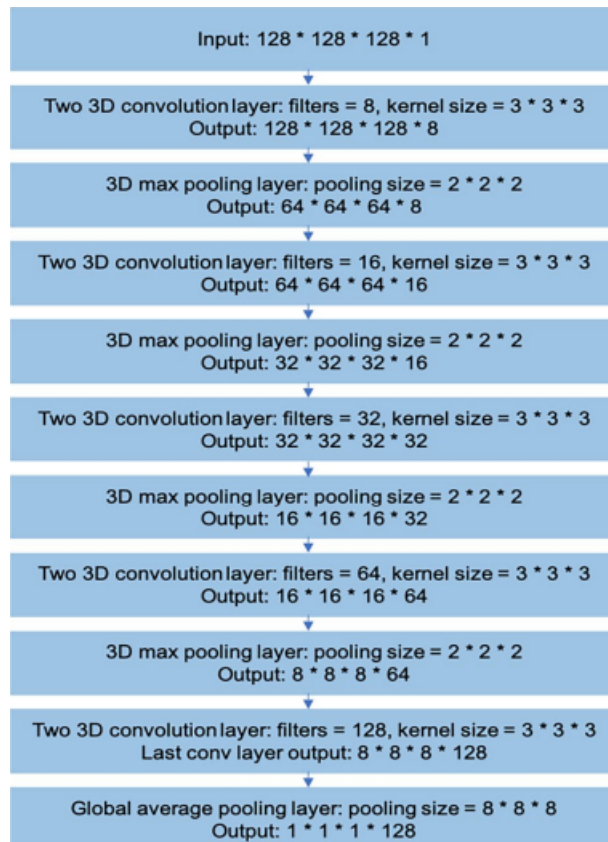


Figure 2.6: Modified 3D VGGNet backbone architecture [105]

Moreover, Zhang et al. [190] have presented a method for detecting and segmenting breast cancer in MRI using a Mask R-CNN model. Trained on non-fat-saturated images and tested on fat-saturated images. The model demonstrates impressive accuracy despite the differences between the training and testing data. It uses a data augmentation strategy that increases generalizability and robustness. The model achieves strong results in terms of Dice similarity coefficient and sensitivity when compared to existing methods. The approach of Zhang et al. could be helpful in clinical practice, offering a tool for automated breast cancer detection that could enhance radiologists' workflow and diagnosis accuracy. The detailed architecture of the Mask R-CNN model used by Zhang et al. [190] is illustrated in Figure 2.7.

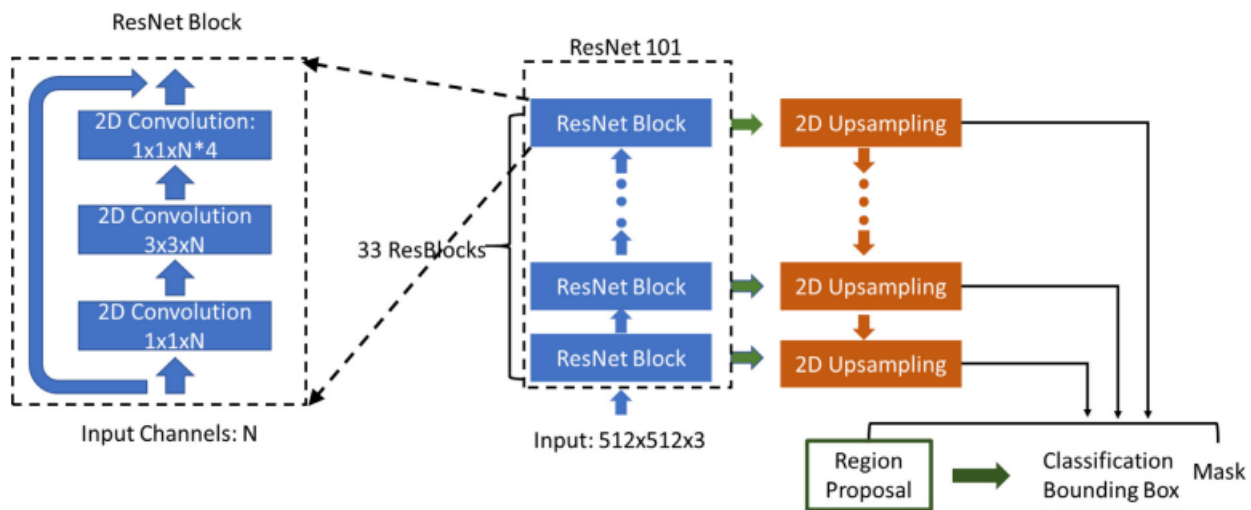


Figure 2.7: Mask R-CNN architecture used in the work of Zhang et al. [190]

2.3.2 Uniparametric data-driven DCE-MRI breast tumor segmentation methods

Within this category of methods, breast tumor segmentation is typically conducted using a single DCE-MRI sequence, most commonly the T1c sequence. These approaches have demonstrated computational simplicity when compared to multiparametric data-driven methods. Nevertheless, a single MRI sequence is often inadequate for capturing the complete morphological characteristics of the tumor under investigation. Furthermore, uniparametric data-driven methods tend to exhibit elevated false positive and false negative rates, primarily due to the resemblance between the enhancement patterns of tumorous and healthy tissues. For example, Hirsch et al. [70] have introduced a deep learning model based on a 3D U-Net convolutional neural network (CNN) to achieve fully automated breast tumor segmentation in MRI scans (see Figure 2.8 for illustration), reaching radiologist-level accuracy. The model was trained on an extensive dataset of over 60,000 clinical MRI scans, which included 2,555 segmented malignant cases and 60,108 benign cases, enabling robust feature extraction and superior generalization. By leveraging volumetric 3D imaging

data rather than the conventional 2D slice-by-slice approach, the model captures complex spatial characteristics of tumors. Additionally, dynamic contrast enhancement (DCE) data and intensity normalization techniques were employed to harmonize imaging features across scans, enhancing segmentation precision. The model achieved a Dice score of 0.77, closely matching radiologists' performance (Dice scores of 0.69 to 0.84). Thus highlighting its potential as an efficient and accurate tool for breast MRI analysis.

Despite these advancements, the model has limitations in handling cases with specific tumor morphologies and dense breast tissue, particularly in patients with high background parenchymal enhancement (BPE), where segmentation accuracy decreases. The MRI protocol used (sagittal plane imaging) also limits direct application in settings favoring axial planes, which are more common in clinical practice. To address these issues, future work could involve training the model on larger, more diverse datasets that include high-resolution, multi-planar images, especially axial plane MRIs, and integrating further optimization techniques to improve accuracy in dense tissue cases. Expanding these capabilities could greatly enhance the model's robustness, clinical applicability, and diagnostic impact in breast imaging.

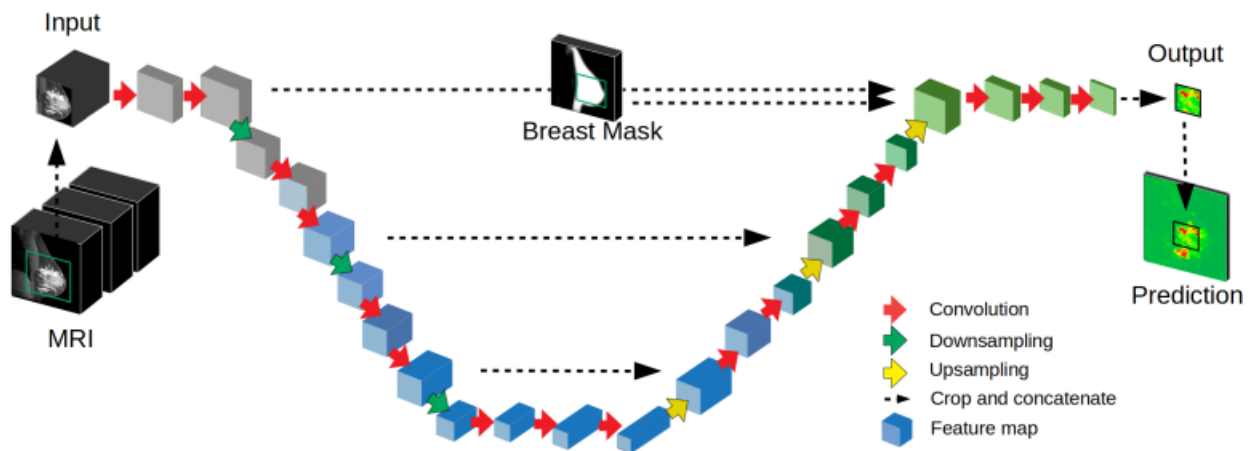


Figure 2.8: Illustration of the 3D U-Net convolutional neural network used for segmentation in the work of Hirsch et al. [70]

In addition, Rehman et al. [146] have proposed EEU-Net, an improved deep learning model for breast tumor segmentation in MRI scans, addressing the challenges of manual segmentation, tumor variability, and computational complexity. EEU-Net enhances the U-Net architecture by integrating Edge Encoder Blocks (EEB) and Edge Guidance Blocks (EGB) to focus on tumor boundaries, improving segmentation accuracy. The model was tested on the RIDER breast MRI dataset using five-fold cross-validation, achieving superior performance compared to state-of-the-art models, with a Dice coefficient of 0.884 and a Jaccard index of 0.804. Its custom loss function combines pixel loss and boundary loss, ensuring precise tumor region identification. Results demonstrate that EEU-Net effectively captures tumor structures and edges, outperforming traditional meth-

ods. Future work aims to apply the model to larger datasets, enhance computational efficiency, and incorporate multi-modal MRI inputs for further improvements in automated breast cancer diagnosis. The architecture of EEU-Net as it is proposed by Rehman et al. [146] is exhibited in Figure 2.9.

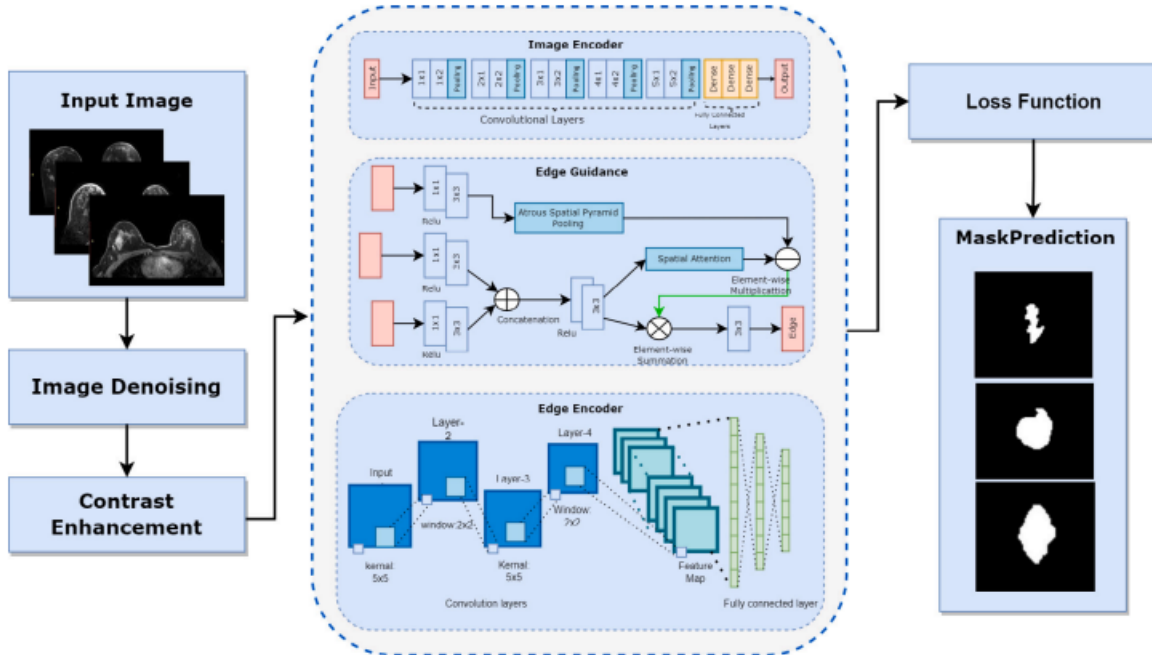


Figure 2.9: Architecture of EEU-Net proposed by Rehman et al. [146]

Furthermore, Wang et al. [172] have proposed a hybrid architecture combining 2D and 3D networks, using a technique called M2D3D-MC. The objective of this work is to combine the computational efficiency of 2D networks with the volumetric representation capabilities of 3D networks. The proposed method, M2D3D-MC, introduces three key contributions: (i) a hybrid 2D–3D convolutional module that addresses the loss of volumetric information inherent in 2D networks by integrating 3D spatial features extracted from adjacent slices; (ii) a multi-scale block designed to mitigate the impact of significant variations in lesion size on segmentation accuracy; and (iii) an image representation reconstruction module to enhance the overall segmentation performance. The M2D3D-MC model was evaluated on a dataset comprising 90 patients and 2,245 annotated axial slices. The method achieved promising results, with a Dice Similarity Coefficient (DSC) of 76.48, Sensitivity (SEN) of 75.93, and Positive Predictive Value (PPV) of 82.40. M2D3D-MC outperformed conventional segmentation models, including 2D U-Net, 3D U-Net, and other widely used approaches, demonstrating superior segmentation accuracy. Notably, the integration of a multi-scale block enabled more effective segmentation of lesions with varying sizes. Nevertheless, a key limitation of this study lies in the relatively small dataset, which may affect the model’s generalizability. Expanding the dataset would likely enhance the robustness and overall performance of the proposed approach.

Moreover, Jiao et al. [81] have exhibited a 2D segmentation method based on U-Net++. The presented method is composed of two steps: in the first step, the whole breast region is segmented from the DEC-MRI image using the U-Net++. In the second step, Faster RCNN is employed to detect the mass like tumor from the produced segmented object of the breast region. The proposed segmentation technique was evaluated using a private dataset consisting of images from 75 patients and subsequently compared to U-Net. The results demonstrated a marginal improvement over U-Net, with performance metrics showing slight gains: Dice Coefficient of 0.951 (versus 0.941 for U-Net), Jaccard Index of 0.908 (versus 0.891 for U-Net), and Sensitivity of 0.948 (versus 0.941 for U-Net). May be this is due to the limited dataset size. Increasing the number of patients in the dataset could improve the generalizability of the method.

2.4 Comparison of the reviewed methods

Each of the reviewed deep learning-based methods exhibits distinct characteristics, each tailored to address specific aspects of tumor segmentation. In this section, we provide a comprehensive comparison of the analyzed studies based on four key criteria: the data dimensionality handled by each approach, the techniques employed, the dataset(s) used for training and evaluation, and the reported results which are presented as stated in the original published works. Specifically, the results are expressed in terms of three evaluation metrics, namely: *accuracy*, *Dice Similarity Coefficient (DSC)*, and *Jaccard index*. Mathematically, these evaluation metrics are formulated using the parameters: *True Positives (TP)*, *True Negatives (TN)*, *False Positives (FP)*, and *False Negatives (FN)*, defined as follows:

- **TP**: refers to the number of correctly segmented contaminated pixels (voxels).
- **TN**: represents the number of correctly segmented uncontaminated pixels (voxels).
- **FP**: designates the number of uncontaminated pixels segmented as contaminated pixels (voxels).
- **FN**: is the number of contaminated pixels segmented as uncontaminated pixels (voxels).

The formulas for the evaluation metrics are given as follows:

$$\text{Accuracy} = \frac{TP + TN}{TP + TN + FP + FN},$$

it measures the overall correctness of the model by considering both correctly segmented contaminated and uncontaminated pixels (voxels).

$$\text{DSC} = \frac{2TP}{2TP + FP + FN},$$

it quantifies the overlap between predicted and ground truth segmentations, with values ranging from 0 (no overlap) to 1 (perfect overlap).

$$\text{Jaccard Index} = \frac{TP}{TP + FP + FN},$$

Also known as the Intersection over Union (IoU), it evaluates the similarity between predicted and actual segmentations.

Table 2.1 summarizes the key characteristics of these methods

Class	Work	Data dimension	Description	Technique(s)	Dataset(s)	Result(s)
Multiparametric data-driven methods	Peng et al. [139] (2022)	3D	Breast tumor segmentation in 3D multi-modal MRI using hierarchical networks and inter-modality information interaction	DenseVoxNet, 3D-TOSN, BD-RSIIM	Private dataset with 590 patients, 3D breast MRI scans (including T1c and T2c images)	DSC: 90.49% (T1c), 85.07% (T1)
	Liu et al. [105] (2021)	Pseudo-3D	Breast tumor prognostic outcome prediction on 3D DCE-MRI	Mask-Guided CNN (3D-VGGNet, CAM, mask-guided attention)	Private dataset with 115 patients (3D DCE-MRI scans)	Accuracy (training: 82.3%, validation: 79.6%)
	Zhang et al. [190] (2022)	3D	Automatic detection and segmentation of breast cancer in MRI	Mask R-CNN (Region-based CNN with Feature Pyramid Network, ResNet-101)	Private dataset with 241 patients (training) and 98 patients (testing). Non-fat-sat MRI for training, fat-sat MRI for testing	Per-slice detection accuracy of 86% (training) and 75% (testing). Per-lesion detection rate: 99.5% (training), 100% (testing). DSC : 82% (training), 79% (testing).
Uniparametric data-driven methods	Hirsch et al. [70] (2020)	3D	Fully automated breast tumor segmentation in MRI using deep learning	3D U-Net, DeepMedic, Conditional Random Field	Large private dataset: 2,555 malignant + 60,108 benign breasts for training and 250 test cases segmented by radiologists	DSC: 77%
	Rehman et al. [146] (2024)	2D	Boundary-driven deep learning for precise segmentation of breast tumors in DCE-MRI	EEU-Net	Public dataset: RIDER breast MRI dataset [rider]	Jaccard Index: 80% and DSC: 88%
	Wang et al. [172] (2021)	Mixed 2D and 3D	Lesion segmentation in breast DCE-MRI	M-2D3D	Private dataset with 90 patients, 2245 annotated axial slices	DSC: 76.48%, better segmentation of varying lesion sizes.
	Jiao et al. [81] (2020)	2D	Deep CNN-based automatic breast segmentation and mass detection in DCE-MRI	U-Net++	Private dataset with 75 patients	DSC: 95%, Jaccard Index: 0.91%

Table 2.1: Comparison of the reviewed methods according to few criteria.

2.5 Synthesis and insights

From Table 2.1, it is evident that most of the reviewed approaches employ full 3D deep learning models. Examples include Peng et al.'s IMIIN, which utilizes DenseVoxNet, as well as 3D-TOSN

and BD-RSIIM. Additionally, Hirsch et al. propose a 3D U-Net-based method, while Zhang et al. implement Mask R-CNN, all of which leverage volumetric data to capture spatial context. In contrast, Liu et al. adopt a pseudo-3D approach, where a 2D CNN is enhanced with 3D contextual cues to predict prognostic outcomes. Meanwhile, Jiao et al. rely on a purely 2D architecture, specifically U-Net++, for segmentation and mass detection. This observation underscores the preference for 3D segmentation over 2D segmentation, as 3D representations provide a more comprehensive spatial perspective and enable the extraction of more discriminative features for tumor characterization.

Moreover, the majority of the reviewed methods were trained and evaluated on private datasets, which vary significantly in size and composition. Hirsch et al. utilized a large dataset comprising over 60,000 scans, facilitating robust training, whereas smaller datasets, such as Jiao et al.'s (75 patients), limit the generalizability of the model. Peng et al.'s dataset, consisting of 590 patients, and Zhang et al.'s 241 training cases provide a moderate-scale dataset; however, they lack standardization. In contrast, only one study leveraged a public dataset, specifically the RIDER breast MRI dataset. Consequently, comparing the performance of the analysed methods remains challenging due to variations in evaluation data. Despite these differences, the majority of approaches employ convolutional autoencoders with diverse architectures, highlighting their relevance in this domain.

Overall, the reviewed methods demonstrate that full 3D models excel in precise tumor delineation due to their ability to leverage volumetric context. In contrast, pseudo-3D and 2D methods can also achieve high effectiveness, particularly when enhanced with attention mechanisms or multi-input strategies, making them suitable for both segmentation and prognostic tasks. The choice of architecture reflects a balance between dataset size, computational complexity, and specific clinical objectives, with each approach exhibiting distinct advantages in terms of accuracy, Dice Similarity Coefficient, Jaccard Index, and overall performance.

As the field of DCE-MRI breast tumor segmentation continues to advance, several promising research directions emerge. The following outlines key perspectives and potential strategies to further enhance this domain. Future efforts should focus on optimizing convolutional autoencoders, exploring alternative deep learning architectures, integrating multiple approaches, and developing novel models to achieve more accurate and efficient segmentation. The following are our suggestions for future works:

- All the reviewed methods were trained on well-aligned, high-quality datasets. To make these approaches more adaptable to real-world clinical settings, future research should focus on developing robust pre-alignment modules and domain adaptation techniques that can handle diverse datasets with varying MRI protocols and modalities.
- Full 3D models deliver great accuracy, but they come with high computational costs. To make them more practical for real-world clinical use, future research could focus on developing

lighter architectures or using efficient training techniques like model pruning and knowledge distillation.

- Hybrid and pseudo-3D approaches hold great potential, but further research is needed to better capture 3D spatial relationships while keeping computational demands manageable.
- Although overall accuracy is high, segmenting small or irregularly shaped tumors remains a challenge. Integrating advanced loss functions, such as boundary-aware or focal loss, along with attention mechanisms designed to capture fine details, could help improve performance.
- The widespread use of private datasets limits reproducibility and comparability across studies. Creating and leveraging large, publicly available datasets would enable cross-validation, standardized benchmarking, and broader clinical adoption.

2.6 Conclusion

In conclusion, this chapter has presented a comprehensive review of DCE-MRI breast tumor segmentation research, focusing on recent state-of-the-art methods aimed at enhancing segmentation accuracy. Through a comparative analysis based on key criteria, we identified the strengths and limitations of existing approaches. This evaluation also outlined promising directions for future research to further advance the field and improve clinical outcomes.

In the next chapter, we will provide the necessary details and descriptions of our main contribution made in the setting of this work, by which we aim to further contribute to the progress in DCE-MRI breast tumor segmentation and ultimately improve patient outcomes.

Chapter 3

RicIU-Net: Rician noise injection in the U-Net Encoder for breast DCE-MRI tumor segmentation

3.1 Introduction

Dynamic Contrast-Enhanced MRI (DCE-MRI) is a key modality for breast tumor detection, but its diagnostic value is often compromised by Rician noise, which degrades image quality and affects segmentation accuracy. While U-Net remains a widely used architecture for medical image segmentation, it is sensitive to such acquisition artifacts.

In this chapter, we introduce RicIU-Net, a robust variant of U-Net designed to improve segmentation performance under noisy conditions. Our approach involves injecting controlled Rician noise into selected Encoder layers during training, enabling the model to learn more discriminative and noise-resilient features. The chapter is organized as follows: Section 3.2 introduces the nature and impact of Rician noise in breast DCE-MRI imaging, emphasizing its detrimental effects on segmentation accuracy. Section 3.3 reviews prior work on noise injection as an augmentation strategy in deep learning, highlighting the gap in its application to breast MRI segmentation. Section 3.4 presents the proposed RicIU-Net model, detailing the rationale for feature-space noise injection and the specific modifications made to the U-Net architecture. Section 3.5 describes the implementation pipeline, dataset characteristics, as well as training and validation of the proposed architecture, and reports the performance of the new RicIU-Net compared with the baseline and a recent U-Net variant. Finally, Section 3.6 concludes the chapter with a summary of the presented contributions.

3.2 Prior work on noise injection as an augmentation technique

3.2.1 Description of existing work

Noise injection into the hidden layers of CNNs has emerged as a powerful augmentation and regularization strategy. By perturbing intermediate representations, such techniques aim to improve generalization, robustness to adversarial attacks, and out-of-distribution (OOD) performance. A notable contribution in this area is the work of He et al. [67] who have proposed *Parametric Noise Injection (PNI)*, where trainable Gaussian noise is added to the weights or activations of a network. When combined with adversarial training, this method led to significant gains in both clean and adversarial accuracy, with improvements of +1.1% and +6.8%, respectively, on CIFAR-10. In parallel, Zhong et al. [195] have introduced the concept of adversarial perturbation in internal activations through the *Adversarial Noise Layer (ANL)* and the *Class Adversarial Noise Layer (CANL)*, focusing on perturbing feature maps rather than inputs. Their technique demonstrated improved robustness while maintaining classification performance.

Further advancing the concept of noise regularization, Levi et al. [99] have proposed the *Noise Injection Node Regularization (NINR)*, a technique that injects structured noise into individual neurons during training. This method outperformed classic regularizers such as Dropout and L2 regularization, especially in scenarios with domain shifts. Moreover, Thapa et al. [167] have investigated the effects of different noise types (*e.g.*, Gaussian, speckle, salt-and-pepper) injected at the input level and observed their impact on CNN performance. Their study revealed that speckle noise is particularly effective at maintaining model robustness, while hidden-layer noise was acknowledged as a complementary approach worth deeper exploration.

On the other side, the work of Hendrycks et al. [68], through the *Many Faces of Robustness* study, systematically has analyzed several augmentation strategies including AugMix, Dropout, and weight noise. Their experiments on calibration and generalization highlighted that noise injected at the weight level, especially when applied beyond the input, improves OOD generalization and calibration reliability. Finally, in a more recent work, Kim et al. [87] have exhibited *Colored Noise Injection (CNI)*, an evolution of PNI that introduces structured, layer-specific noise during training. Unlike independent Gaussian noise, CNI correlates perturbations across layers, leading to increased robustness without sacrificing accuracy on clean data.

3.2.2 Gap in the literature and motivation

Despite the diversity of the aforementioned contributions, the vast majority of noise injection techniques have been developed and evaluated primarily in the context of image classification tasks. Applications to more complex problems such as medical image segmentation remain relatively

unexplored. In particular, to the best of our knowledge, no prior work has explicitly investigated the use of hidden-layer noise injection as an augmentation strategy for DCE-MRI in the context of breast tumor segmentation.

Given the critical importance of accurate lesion delineation in DCE-MRI for diagnosis, treatment planning, and monitoring, there is a clear opportunity to explore the potential of such techniques in this domain. The present work aims to address this gap by introducing and evaluating a novel noise injection strategy applied within the hidden layers of a convolutional neural architecture, specifically tailored for 2D breast DCE-MRI tumor segmentation. Our hypothesis is that this strategy can improve the model’s ability to learn robust, discriminative features by reducing overfitting to noise-free training distributions and enhancing generalization to variable imaging conditions.

3.3 Rician noise in breast DCE-MRI: Characteristics and impact

3.3.1 Rician noise

Rician noise is precisely characterized by its probability density function, which describes the distribution of signal magnitudes in MRI arising from thermal noise:

$$f_R(r, \sigma, \sigma_n) = \frac{r}{\sigma_n^2} \exp\left(-\frac{r^2 + \sigma^2}{2\sigma_n^2}\right) I_0\left(\frac{r\sigma}{\sigma_n^2}\right),$$

where r denotes the signal magnitude, σ represents the true signal amplitude, and σ_n is the standard deviation of the noise.

Rician noise is the preferred model for simulating realistic conditions in breast MRI due to two principal factors:

- On one hand, in DCE-MRI, thermal noise in raw complex data is Gaussian. However, the non-linear transformation during magnitude image reconstruction inherently converts this into a Rician distribution. Consequently, Rician noise accurately models the statistical properties of noise observed in clinical breast MRI magnitude images.
- On the other hand, Rician noise, unlike the Gaussian, demonstrates signal-dependent behavior. Its distribution varies with underlying signal intensity; it approaches a Rayleigh distribution in low SNR regions and approximates a Gaussian distribution in high SNR areas. This dependency is crucial for realistic simulation across the diverse signal intensities within a breast MRI image.

3.3.2 Detrimental effects of Rician noise on breast MRI images

The presence of Rician noise in breast DCE-MRI images introduces several significant challenges that can impede accurate diagnosis and subsequent image processing:

- Rician noise introduces a *signal-dependent bias*, particularly pronounced in low SNR regions. This bias artificially elevates signal intensities in areas with genuinely low signal, leading to a reduction in image contrast. In breast DCE-MRI, this phenomenon can obscure subtle lesions, making their differentiation from healthy tissue or background noise considerably more challenging.
- Rician noise manifests as random fluctuations in pixel intensities, resulting in a *grainy or speckled appearance*. This directly diminishes the perceived visual quality of the image, complicating the interpretation of anatomical details and the identification of abnormalities by radiologists. Such degradation can obscure vital diagnostic information and diminish diagnostic confidence.
- The inherent bias from Rician noise can lead to inaccuracies in quantitative metrics derived from breast MRI, such as tumor size, enhancement kinetics in DCE-MRI, and diffusion parameters in diffusion-weighted imaging. These quantitative assessments are critical for precise diagnosis, treatment planning, and monitoring therapeutic responses. Inaccurate measurements due to noise can result in mischaracterization of lesions or suboptimal clinical decisions.
- The signal-dependent and non-Gaussian nature of Rician noise complicates its removal or mitigation using conventional denoising algorithms, which often presuppose Gaussian noise. This significantly impacts subsequent image processing steps, including segmentation, registration, and feature extraction, which are fundamental to computer-aided diagnosis (CAD) systems. Noisy images can produce imprecise segmentation boundaries, affecting the accuracy of tumor volume estimation and shape analysis.

3.4 Proposed model: RicIU-Net

The proposed model, herein called: *Rician-Injected U-Net (RicIU-Net)*, builds upon the standard U-Net architecture, which is widely adopted for medical image segmentation tasks due to its Encoder-Decoder structure and skip connections. For a comprehensive description of the baseline U-Net architecture, the reader is referred to Subsection 1.5.2.2 of Chapter 1. In this section, we introduce the principal innovation of the RicIU-Net: a feature-space Rician noise injection mechanism incorporated during training to enhance model robustness and generalization under noisy clinical imaging conditions. The architecture of the RicIU-Net presented is illustrated in Figure ?? and its detailed descriptions are given in the following subsections.

3.4.1 Feature-space Rician noise injection

The core methodological contribution of the new RicIU-Net is the injection of synthetic Rician noise into the intermediate feature representations generated by the Encoder during training. Unlike conventional data-augmentation approaches that perturb the input domain, this technique perturbs the internal representational space, thereby promoting the acquisition of noise-invariant and semantically rich features.

Let F_l denote the feature map output by Encoder layer l . The perturbed feature map \tilde{F}_l is defined as:

$$\tilde{F}_l = \sqrt{(F_l + n_r)^2 + n_i^2}, \quad (3.1)$$

where n_r and n_i are independent Gaussian noise tensors with zero mean and standard deviation σ , representing the real and imaginary components of complex Gaussian noise, respectively. This formulation effectively models Rician-distributed noise, which is characteristic of magnitude MRI images subject to thermal fluctuations.

Noise is introduced only during the training phase and is not applied during inference, thus preserving prediction fidelity. At each training iteration, Encoder layers for noise injection are randomly selected to ensure robustness across multiple representational depths. The noise intensity σ is treated as a hyperparameter, allowing the model to be calibrated to varying levels of image degradation.

3.4.2 Rationale for feature-space noise injection

Feature-space noise injection offers several theoretical and empirical advantages over input-level perturbations. Firstly, it preserves the anatomical and structural consistency of input images, which is critical for accurate medical segmentation. Secondly, perturbing internal representations allows the network to experience a broader spectrum of degradation patterns, encouraging the learning of noise-resilient abstractions. Finally, this method introduces an implicit regularization effect that mitigates overfitting to clean training data, a phenomenon particularly relevant when datasets are limited in size or variability.

This strategy is aligned with previous findings that demonstrate that injecting noise into intermediate network representations improves robustness and generalization [12, 124]. By disrupting the latent space during optimization, the model is forced to rely on stable, task-relevant features that are less sensitive to superficial distortions.

3.4.3 Motivation for Encoder-only noise injection

A key design decision in the RicIU-Net architecture is to restrict noise injection exclusively to the Encoder pathway. This choice is grounded in the distinct functional roles of the Encoder and Decoder within U-Net. The Encoder is responsible for extracting high-level semantic features from the input, while the Decoder reconstructs spatial detail and produces the final segmentation mask. Hence, the perturbation of the Encoder fosters the development of robust, noise-invariant features, which are essential for reliable downstream segmentation. In contrast, injecting noise into the Decoder would risk compromising the integrity of the reconstructed spatial information, potentially leading to degraded boundary delineation and reduced accuracy.

Additionally, given that skip connections already transfer fine-grained information from the Encoder to the Decoder, it is imperative to maintain these signals in a relatively uncorrupted state to preserve anatomical fidelity. From an optimization perspective, limiting perturbations to the Encoder stabilizes the training process and avoids direct interference with the segmentation output layer.

As can be seen in Figure 3.1, the proposed architecture RicIU-Net consists of an input layer, four encoding blocks, a central deep convolutional block, followed by four decoding blocks and a two-channel output layer. Rician noise is injected exclusively into the fourth Encoder block and the central block (block 5), with a noise level of $\sigma = 0.05$. This latter configuration has been selected based on an empirical evaluation of several noise injection strategies, which varied both the number of perturbed Encoder layers (*i.e.* including perturbation of all Encoder layers, only the early layers, or only the deeper layers) and the noise scheduling schemes (*i.e.* including fixed α values, increasing α with depth, and decreasing α with depth). Among the tested configurations, the selected strategy consistently yielded the most favorable segmentation performance. These results suggest that targeted perturbation of deeper encoder representations strikes a balance between regularization and feature discriminability.

3.4.4 RicIU-Net *vs.* baseline U-Net: Expected improvements

The proposed modification to the U-Net architecture, which involves the controlled injection of Rician noise into Encoder feature maps during training, is expected to offer several key advantages, particularly in the context of noisy clinical MRI data.

- First, this approach is expected to improve the *robustness* of the model by simulating real-world acquisition artifacts. Exposure to such noise during training should help the network develop resilience to signal degradation commonly encountered in clinical imaging.
- Second, by perturbing intermediate feature representations, the model is expected to learn more *discriminative and noise-invariant features*, thereby enhancing its ability to accurately

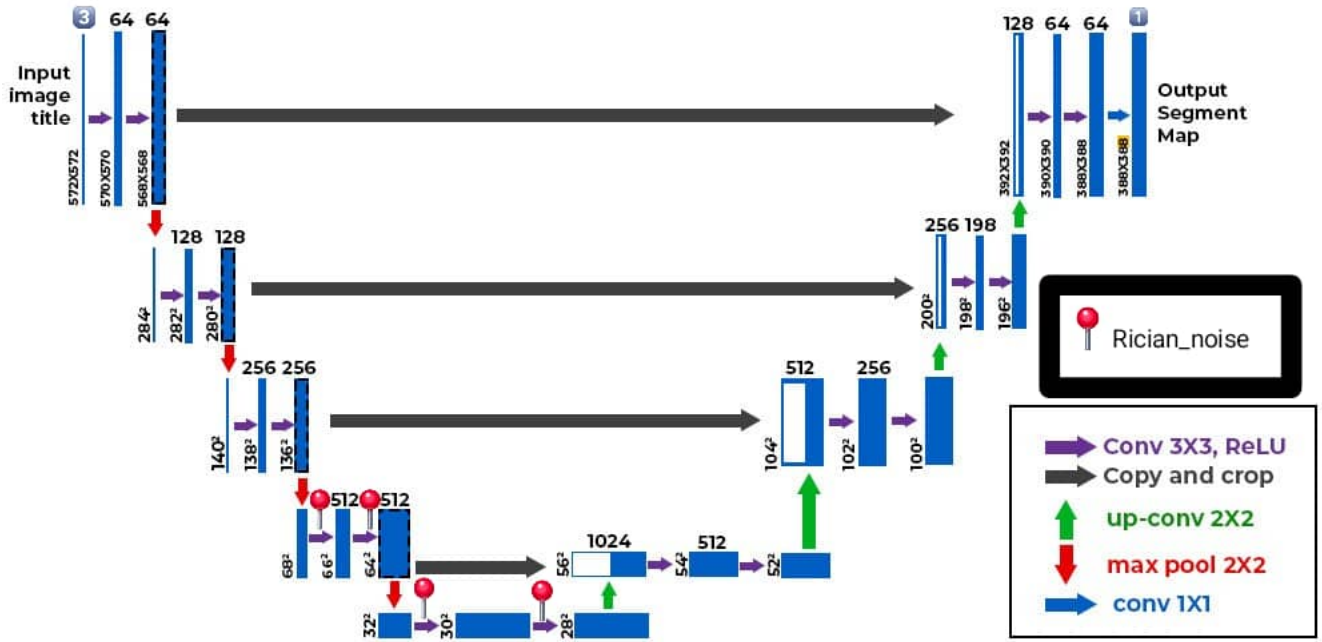


Figure 3.1: Illustration of the architecture of the proposed RicIU-Net.

segment relevant structures even under suboptimal image quality conditions. This is hypothesized to result in improved *generalization performance*, particularly when applied to heterogeneous or previously unseen datasets.

- Third, noise injection is expected to function as an effective form of *implicit regularization*, minimizing overfitting to clean training data. By introducing controlled variability through synthetic noise, the training process can emulate a wider range of imaging scenarios without requiring additional annotated data.
- Finally, these enhancements are expected to translate into improved segmentation performance, as measured by quantitative metrics such as the Dice similarity coefficient, particularly in settings where input images exhibit significant noise.

These hypotheses will be empirically validated by comparative experiments against a baseline U-Net model, using a real-world breast DCE-MRI dataset.

3.5 Implementation and evaluation

3.5.1 Experimental dataset

The subsections below describe the dataset used in this study, as well as how this latter has been prepared for the training, validation, and test of the presented RicIU-Net architecture.

3.5.1.1 Dataset description

For training and evaluation of the RicIU-Net model, we have used the publicly available BreastDM data set [194], which is composed of breast DCE-MRI images offering high-resolution visualization of breast tissues and tumor regions, each associated with a manually annotated segmentation mask provided by medical experts. The main characteristics of the dataset are summarized as follows:

- **Format of the images:** The DCE-MRI images are in the RGB format with varying resolutions, resized to a uniform size of 256×256 pixels to facilitate training.
- **Number of images:** After a cleaning operation of the dataset, 29512 images in total are remained, divided into 20434 images for training, 1989 images for validation, and 7089 images for testing.
- **Format of the segmentation masks:** The binary masks are also in 256×256 pixels of size. They indicate the presence of a tumor (resp. tumors) within the associated DCE-MRI images, where their foreground (representing the tumor(s)) is labeled as 1 and their background as 0.
- **Organization of the data:** The dataset is essentially partitioned into three distinct subsets, namely: a training set (used to train the model parameters), a validation set (used to monitor model performance and prevent overfitting) and a test set (used to objectively evaluate generalization performance).

3.5.1.2 Dataset preparation

Before training, all input images of the dataset were normalized to the $[0,1]$ range to ensure consistent intensity scaling and facilitate numerical stability across the dataset. To improve the model's ability to generalize and better reflect real-world variability, a data augmentation strategy was employed that included random rotations and flips to introduce spatial diversity.

3.5.2 Development environment and tools

For this project focused on the segmentation of breast cancer tumors from medical images, the development environment used is Google Colab Pro. This cloud-based platform provides computing power well-suited to the needs of deep learning, notably through access to GPU/TPU resources that significantly accelerate model training.

Furthermore, the dataset is loaded directly from Google Drive. This approach ensures quick and secure access to datasets stored in the cloud and facilitates the automatic saving of models and intermediate results.

Moreover, the entire project is implemented using the Python programming language, which is a standard in artificial intelligence due to its simplicity and its extensive ecosystem of specialized libraries. Among these latter, we have mainly used:

- TensorFlow : for building, compiling, and training deep learning models.
- NumPy: for managing multidimensional arrays and performing numerical operations.
- OpenCV: for image processing and manipulation.
- Matplotlib: for visualizing results such as images, masks, and training curves.
- os: for file handling and navigation within the directory structure.

Layer (type)	Output Shape	Param #	Connected to
input_layer (InputLayer)	(None, 256, 256, 3)	0	-
lambda (Lambda)	(None, 256, 256, 3)	0	input_layer[0][0]
conv2d (Conv2D)	(None, 256, 256, 64)	1,792	lambda[0][0]
batch_normalization (BatchNormalizatio...	(None, 256, 256, 64)	256	conv2d[0][0]
dropout (Dropout)	(None, 256, 256, 64)	0	batch_normalizat...
conv2d_1 (Conv2D)	(None, 256, 256, 64)	36,928	dropout[0][0]
batch_normalizatio... (BatchNormalizatio...	(None, 256, 256, 64)	256	conv2d_1[0][0]
lambda_1 (Lambda)	(None, 256, 256, 64)	0	batch_normalizat...
max_pooling2d (MaxPooling2D)	(None, 128, 128, 64)	0	lambda_1[0][0]
conv2d_2 (Conv2D)	(None, 128, 128, 128)	73,856	max_pooling2d[0]...
batch_normalizatio... (BatchNormalizatio...	(None, 128, 128, 128)	512	conv2d_2[0][0]

Figure 3.2: Illustration of an implemented part of RicIU-Net’s Encoder.

An overview of the implemented architecture is given in Figures 3.2 and 3.3.

3.5.3 RicIU-Net training and validation

The performance of the RicIU-Net model was evaluated using several performance metrics in the training, validation, and test sets. The evaluation has been carried out in 60 epochs out of 150,

conv2d_15 (Conv2D)	(None, 128, 128, 128)	147,584	dropout_7[0][0]
batch_normalizatio... (BatchNormalizatio...)	(None, 128, 128, 128)	512	conv2d_15[0][0]
conv2d_transpose_3 (Conv2DTranspose)	(None, 256, 256, 64)	32,832	batch_normalizat...
concatenate_3 (Concatenate)	(None, 256, 256, 128)	0	conv2d_transpose... lambda_1[0][0]
conv2d_16 (Conv2D)	(None, 256, 256, 64)	73,792	concatenate_3[0]...
batch_normalizatio... (BatchNormalizatio...)	(None, 256, 256, 64)	256	conv2d_16[0][0]
dropout_8 (Dropout)	(None, 256, 256, 64)	0	batch_normalizat...
conv2d_17 (Conv2D)	(None, 256, 256, 64)	36,928	dropout_8[0][0]
batch_normalizatio... (BatchNormalizatio...)	(None, 256, 256, 64)	256	conv2d_17[0][0]
conv2d_18 (Conv2D)	(None, 256, 256, 1)	65	batch_normalizat...

Total params: 31,055,297 (118.47 MB)
Trainable params: 31,043,521 (118.42 MB)
Non-trainable params: 11,776 (46.00 KB)

Figure 3.3: Illustration of an implemented part of RicIU-Net’s Decoder.

using a learning rate dynamically adjusted by *ReduceLROnPlateau* that has shown the value of 6.25×10^{-6} in epoch 60. The performance evaluation includes: Dice Similarity Coefficient (DSC), Intersection over Union (IoU), Precision, Recall, and Dice loss as a loss function. For illustration, Figure 3.4 (resp. Figure 3.5) shows the evolution of the DSC metric (resp. the Dice loss) through the epochs during training and validation phases. Table 3.1 then summarizes the best results obtained for all the used metrics.

Metric	Training	Validation
DSC	0.8921	0.6325
Precision	0.9142	0.7483
Recall	0.8743	0.6052
Dice loss	0.1097	0.3703

Table 3.1: Summary of RicIU-Net model performance at epoch 60 for training and validation phases.

Generally, RicIU-Net shows strong initial performance with DSC of 0.8921, Precision of 0.9142, and Recall of 0.8743 on the training set. While a gap exists with the validation set (DSC of 0.6325, Precision of 0.7483, and Recall of 0.6052), this highlights clear opportunities for future enhancement. The current Dice loss values, 0.1097 on training and 0.3703 on validation, provide

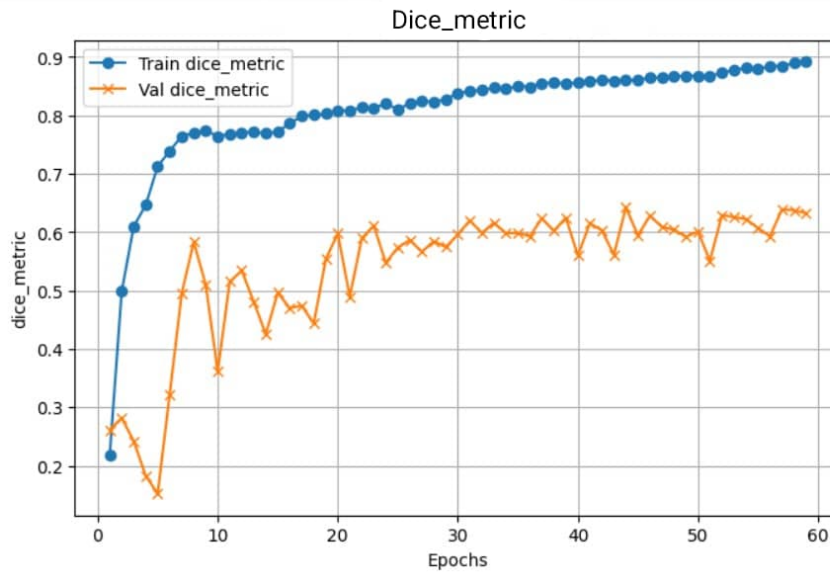


Figure 3.4: Trend of the DSC for training and validation across epochs.

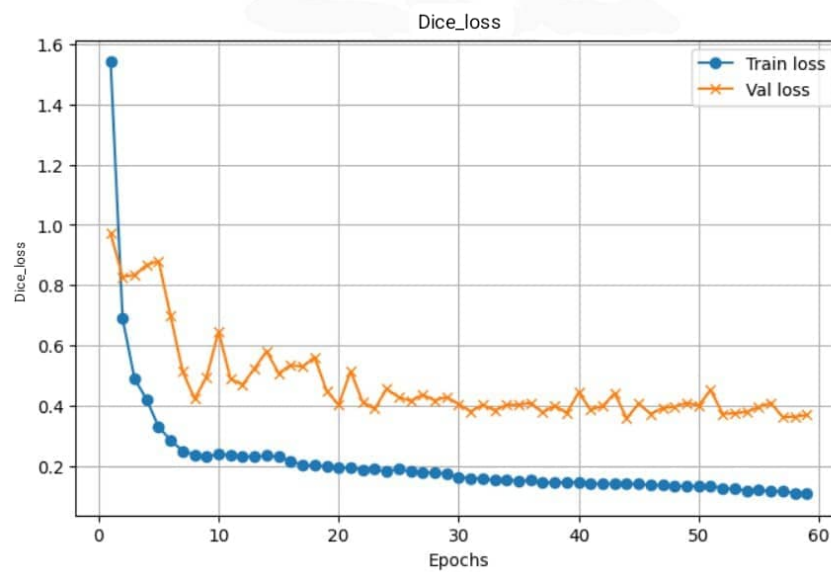


Figure 3.5: Trend of the Dice loss for training and validation across epochs.

a solid baseline. The observed lower recall on validation points to specific areas for improving comprehensive tumor region capture, underscoring the model’s significant potential with continued optimization.

3.5.4 Evaluation of RicIU-Net and comparison with existing methods

A comparative analysis of segmentation performance has been performed between the proposed RicIU-Net and two concurrent methods: standard U-Net [150] and U-Net2.1D [11], and the results obtained are presented in Table 3.2. Specifically, the evaluation was carried out in the training,

validation, and test phases using the same dataset (*i.e.* BreastDM) as used in the benchmark study by Bilic and Chen [11], ensuring a fair and consistent comparison. As reported in that benchmark, the DSC for the standard U-Net and U-Net2.1D models reached 0.49 and 0.60, respectively. In contrast, the proposed RicIU-Net achieved a superior DSC of 0.62, along with an IoU of 0.72 and a minimized segmentation loss of 0.38. These results demonstrate a consistent performance improvement, highlighting the efficacy of the proposed feature space Rician noise regularization strategy in improving segmentation quality. Notably, RicIU-Net outperforms the benchmarked U-Net variants without relying on architectural complexity, suggesting its potential as a lightweight yet effective enhancement to standard Encoder–Decoder models.

For visual illustration, Figures 3.6, 3.7, and 3.8 present the segmentation results produced by the proposed RicIU-Net in three representative cases: a small tumor, a medium-sized tumor, and a large tumor presenting, either a roundish or an irregular (speculated) boundary. As observed, the predicted masks closely match the ground truth in terms of shape, boundary definition, and spatial extent. These visual results qualitatively confirm the model’s ability to accurately delineate tumor regions in varying tumor sizes and morphologies in DCE-MRI breast images.

Evaluated model	DSC	Dice loss	IoU
Baseline U-Net2D (2015)[150]	0.49	/	/
U-Net2.1D (2024)[11]	0.60	/	/
RicIU-Net (proposed)	0.62	0.38	0.72

Table 3.2: Comparison of performance metrics between RicIU-Net and existing methods.

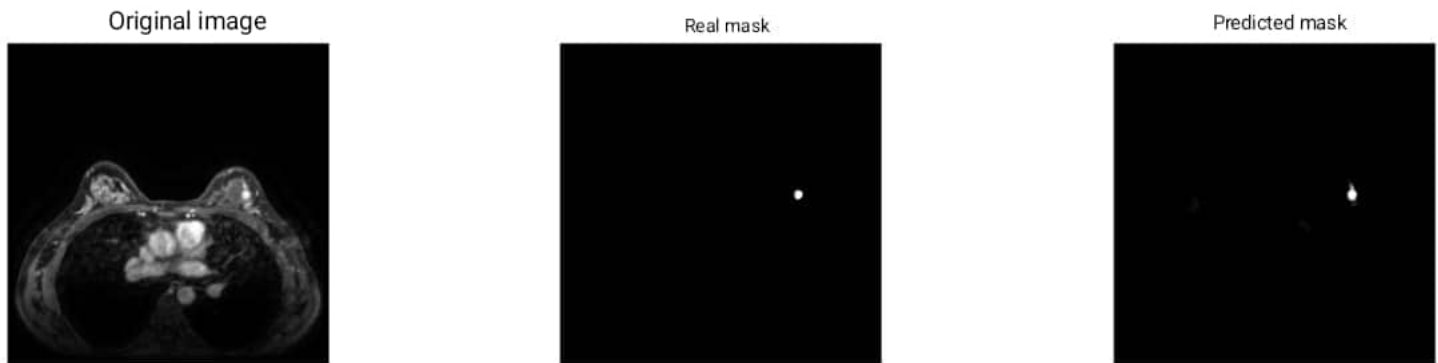


Figure 3.6: Example of the segmentation obtained by the proposed RicIU-Net for a small breast tumor.

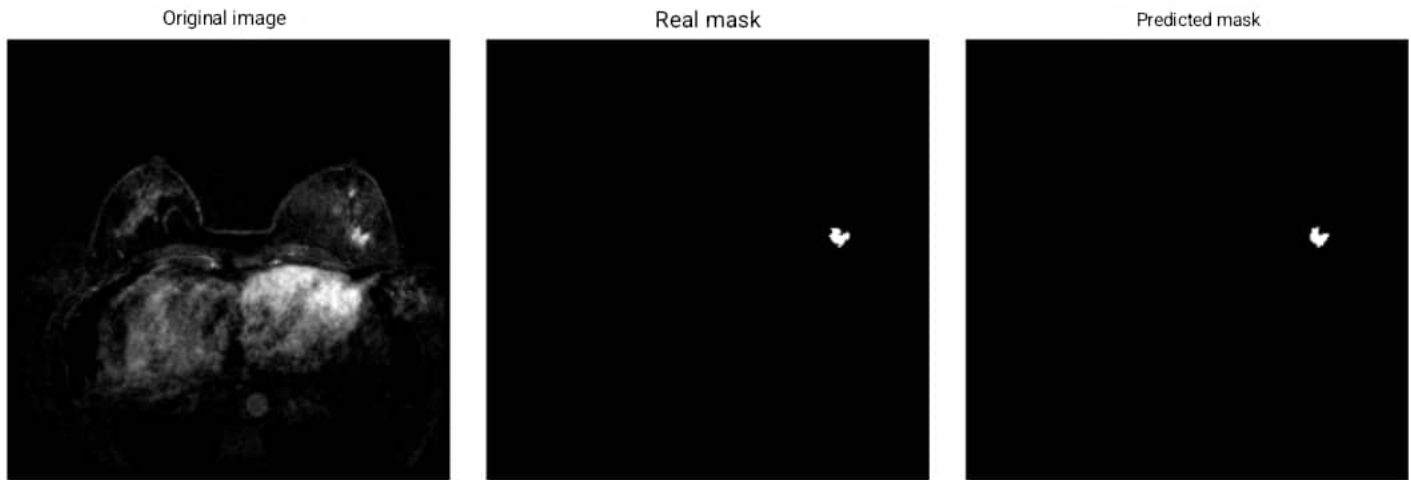


Figure 3.7: Example of the segmentation obtained by the proposed RicIU-Net for a medium-sized breast tumor.



Figure 3.8: Example of the segmentation obtained by the proposed RicIU-Net for a large breast tumor.

3.6 Conclusion

This work introduced RicIU-Net, an enhanced variant of the U-Net architecture, specifically designed to improve robustness in breast tumor segmentation under Rician noise conditions commonly present in DCE-MRI. By selectively injecting Rician noise into deeper Encoder layers during training, the model is encouraged to learn more pertinent and discriminative features, rather than overfitting to noise or low-level artifacts. The proposed method outperforms both the standard U-Net and one of its recent variants, achieving superior quantitative results and visually coherent segmentations. These findings underscore the importance of incorporating acquisition-related

artifacts into the training process to develop more resilient, generalizable, and clinically viable segmentation models.

General conclusion

The integration of artificial intelligence into medical imaging, particularly for the analysis of breast tumors, represents an important step forward in modern medicine. Throughout this work, we have shown how deep learning architectures, especially convolutional neural networks such as U-Net, can significantly improve the automation of medical image segmentation and contribute to more accurate and reliable diagnoses.

This work addresses a central challenge in medical image analysis: the robustness of breast tumor segmentation models in the presence of intrinsic noise in DCE-MRI images, particularly Rician noise. This noise can significantly degrade the image quality and limit the effectiveness of models trained under ideal, noise-free conditions. To overcome this limitation, we introduced an original solution: Rician-Injected U-Net (RicIU-Net), a modified version of U-Net that injects controlled Rician noise into the deeper layers of the encoder during training. This approach encourages the model to learn more robust and discriminative features, making it better adapted to the variability and imperfections of real-world medical imaging.

The experimental analysis carried out in this study demonstrated the superiority of RicIU-Net compared to the classical U-Net and its recent variant U-Net2.1D, particularly on the BreastDM benchmark dataset. The performance gains observed in terms of Dice Score and Intersection over Union (IoU) highlight the effectiveness of our noise injection strategy within the feature space. Notably, these improvements were achieved without relying on any external denoising techniques, emphasizing the strength and robustness of the proposed approach.

Nonetheless, the findings of this work also open up several promising avenues for future research. These include adapting the model to three-dimensional (3D) data, extending its application to other medical imaging modalities, and exploring its deployment in resource-constrained environments. Further improvements could involve the integration of attention mechanisms or the use of transfer learning strategies to enhance generalization. Additionally, ethical aspects related to medical data privacy and algorithmic transparency should be carefully considered in future developments.

Bibliography

- [1] D. Abdelhafiz, C. Yang, R. Ammar, and S. Nabavi. “Deep Convolutional Neural Networks for Mammography: Advances, Challenges and Applications”. In: *BMC Bioinformatics* 20 (2019), pp. 1–20.
- [2] R. Achanta, A. Shaji, K. Smith, A. Lucchi, P. Fua, and S. Susstrunk. “SLIC Superpixels Compared to State-of-the-Art Superpixel Methods”. In: *IEEE Transactions on Pattern Analysis and Machine Intelligence* 34 (2012), pp. 2274–2282.
- [3] R. Adams and L. Bischof. “Seeded Region Growing”. In: *IEEE Transactions on Pattern Analysis and Machine Intelligence* 16 (1994), pp. 641–647.
- [4] S. C. Agner, J. Xu, and A. Madabhushi. “Spectral Embedding Based Active Contour (SEAC) for Lesion Segmentation on Breast Dynamic Contrast Enhanced Magnetic Resonance Imaging”. In: *Medical Physics* 40 (2013), p. 032305.
- [5] S. Amiri, M. M. Movahedi, K. Kazemi, and H. Parsaei. “An Automated MR Image Segmentation System Using Multi-Layer Perceptron Neural Network”. In: *Journal of Biomedical Physics & Engineering* 3.4 (2013), pp. 115–122.
- [6] S. S. Al-amri, N. V. Kalyankar, and S. D. Khamitkar. “Image Segmentation by Using Edge Detection”. In: *International Journal on Computer Science and Engineering* 02 (2010), pp. 804–807.
- [7] R. Azmi, R. Anbiaee, N. Norozi, L. Salehi, and A. Amirzadi. “A New Interactive Self-Training Approach to Segmentation Suspicious Lesions in Breast MRI”. In: *Journal Medical Signals Sensors* 1 (2011), pp. 138–148.
- [8] J. Besag. “On the Statistical Analysis of Dirty Pictures”. In: *Journal of the Royal Statistical Society: Series B (Methodological)* 48 (1986), pp. 259–279.
- [9] S. Beucher. “The Watershed Transformation Applied to Image Segmentation”. In: *Scanning Microscopy* 28 (1992).
- [10] R. Bilal, B. M. Khan, and R. Young. “Breast Cancer Detection and Diagnosis”. In: *Emerging Developments and Practices in Oncology*. Ed. by I. El Naqa. 1st. Michigan: IGI Global, 2018, pp. 1–27.
- [11] A. Bilic and C. Chen. “BC-MRI-SEG: A Breast Cancer MRI Tumor Segmentation Benchmark”. In: *12th International Conference on Healthcare Informatics (ICHI)*. 2024, pp. 674–678.
- [12] C. M. Bishop. “Training with Noise is Equivalent to Tikhonov Regularization”. In: *Neural Computation* 7.1 (1995), pp. 108–116.

- [13] F. Bloch and E. M. Purcell. “Nuclear Induction”. In: *Physical Review* 70.7-8 (1946), pp. 460–474.
- [14] F. Bouchebbah. “A New Levels Propagation Approach to Image Segmentation: Theory and Its Application to 2D/3D Breast MR Images”. PhD thesis in Computer Science. University of Bejaia, July 2020.
- [15] F. Bouchebbah and H. Slimani. “3D Automatic Levels Propagation Approach to Breast MRI Tumor Segmentation”. In: *Expert Systems with Applications* 165 (2021), p. 113965. ISSN: 0957-4174.
- [16] F. Bouchebbah and H. Slimani. “Levels Propagation Approach to Image Segmentation: Application to Breast MR Images”. In: *Journal of Digital Imaging* 32 (2019), pp. 433–449.
- [17] M. Boudiab and H. Bensassi. “Approche à Base d’Alliances dans les Graphes pour la Réduction de la Saturation et de la Congestion dans les Réseaux LTE”. MA thesis. Département d’Informatique, Université de Béjaia, Juillet 2019.
- [18] F. Bozkurt, C. Köse, and A. Sari. “An Inverse Approach for Automatic Segmentation of Carotid and Vertebral Arteries in CTA”. In: *Expert Systems with Applications* 93 (2018), pp. 358–375.
- [19] F. Bray, J. Ferlay, I. Soerjomataram, R. L. Siegel, L. A. Torre, and A. Jemal. “Global Cancer Statistics 2022: GLOBOCAN Estimates of Incidence and Mortality Worldwide for 36 Cancers in 185 Countries”. In: *CA: A Cancer Journal for Clinicians* 72.3 (2022), pp. 209–249.
- [20] R. C. Brigham, R. D. Dutton, T. W. Haynes, and S. T. Hedetniemi. “Powerful Alliances in Graphs”. In: *Discrete Mathematics* 309 (2009), pp. 2140–2147.
- [21] L. A. Brinton, M. M. Gaudet, and G. L. Gierach. *Cancer Epidemiology and Prevention*. 4th. New York: Oxford University Press, 2018, pp. 861–888.
- [22] K. Broelemann, X. Jiang, and A. Schwering. “Automatic Understanding of Sketch Maps Using Context-Aware Classification”. In: *Expert Systems with Applications* 45 (2016), pp. 195–207.
- [23] K. S. Camilius and V. K. Govidan. “A Review on Graph Based Segmentation”. In: *International Journal of Image* 5 (2012), pp. 1–13.
- [24] J. Canny. “A Computational Approach to Edge Detection”. In: *IEEE Transactions on Pattern Analysis and Machine Intelligence* 8 (1986), pp. 679–698.
- [25] J. S. Cardoso and L. Corte-Real. “Toward a Generic Evaluation of Image Segmentation”. In: *IEEE Transactions on Image Processing* 14 (2005), pp. 1772–1782.
- [26] A. Chakravarty and J. Sivaswamy. “RACE-Net: A Recurrent Neural Network for Biomedical Image Segmentation”. In: *Journal of Biomedical and Health Informatics* 23.3 (2018), pp. 1151–1162.
- [27] J. Chen, Y. Lu, Q. Yu, et al. *TransUNet: Transformers Make Strong Encoders for Medical Image Segmentation*. arXiv preprint arXiv:2102.04306. 2021.
- [28] Jieneng Chen, Jieru Mei, Xianhang Li, Yongyi Lu, Qihang Yu, Qingyue Wei, Xiangde Luo, Yutong Xie, Ehsan Adeli, Yan Wang, et al. “TransUNet: Rethinking the U-Net Architecture Design for Medical Image Segmentation Through the Lens of Transformers”. In: *Medical Image Analysis* 97 (2024), p. 103280.

- [29] P. C. Chen and T. Pavlidis. “Image Segmentation as an an Estimation Problem”. In: *Computer Graphics and Image Processing* 12 (1980), pp. 153–172.
- [30] W. Chen, M. L. Giger, and U. Bick. “A Fuzzy C-Means (FCM)-Based Approach for Computerized Segmentation of Breast Lesions in Dynamic Contrast-Enhanced MR Images”. In: *Academic Radiology* 13 (2006), pp. 63–72.
- [31] Y. Chen, S. Ma, X. Chen, and P. Ghamisi. “Hyperspectral Data Clustering Based on Density Analysis Ensemble”. In: *Remote Sensing Letters* 8 (2017), pp. 194–203.
- [32] S. R. Cherry and M. Dahlbom. *PET: Physics, Instrumentation, and Scanners*. 1st. New York: Springer, 2006.
- [33] K. Chockley and E. Emanuel. “The end of radiology ? three threats to the future practice of radiology”. In: *Journal of the American College of Radiology* 13 (2016), pp. 1415–1420.
- [34] D. Cokuslu, K. Erciyas, and O. Dagdeviren. “A Dominating Set Based Clustering Algorithm for Mobile Ad Hoc Networks”. In: *International Conference on Computational Science Berlin, Heidelberg*. Springer, 2006, pp. 571–578.
- [35] *More Edge Detection (Web Resource)*. <https://www.owlnet.rice.edu/~elec539/Projects97/morphjrks/moreedge.html>. (Accessed: 24/06/2025).
- [36] T. Cover and P. Hart. “Nearest Neighbor Pattern Classification”. In: *IEEE Transactions on Information Theory* 13 (1967), pp. 21–27.
- [37] Y. Cui, Y. Tan, B. Zhao, L. Liberman, R. Parbhu, J. Kaplan, M. Theodoulou, C. Hudis, and L. H. Schwartz. “Malignant Lesion Segmentation in Contrast-Enhanced Breast MR Images Based on the Marker-Controlled Watershed”. In: *Medical Physics* 36 (2009), pp. 4359–4369.
- [38] E. Dam, M. Loog, and M. Letteboer. “Integrating Automatic and Interactive Brain Tumor Segmentation”. In: *17th International Conference on Pattern Recognition*. IEEE, 2004, pp. 790–793.
- [39] *Damadian’s Invention (Image)*. https://commons.wikimedia.org/wiki/File:Damadian_invention.jpg. (Accessed : 24/06/2025).
- [40] R. Damadian. “Tumor Detection by Nuclear Magnetic Resonance”. In: *Science* 171 (1971), pp. 1151–1153.
- [41] R. Damadian. “Tumor Detection by Nuclear Magnetic Resonance”. In: *Science* 171.3976 (1971), pp. 1151–1153.
- [42] K. Deb, A. Pratap, S. Agarwal, and T. Meyarivan. “A Fast and Elitist Multi-Objective Genetic Algorithm: NSGA-II”. In: *IEEE Transactions on Evolutionary Computation* 6 (2002), pp. 182–197.
- [43] J. L. Deneubour, S. Aron, S. Goss, and J. M. Pasteels. “The Self-Organizing Exploratory Pattern of the Argentine Ant”. In: *Journal of Insect Behavior* 3 (1990), pp. 159–168.
- [44] A. Dosovitskiy, L. Beyer, A. Kolesnikov, et al. *An Image is Worth 16x16 Words: Transformers for Image Recognition at Scale*. arXiv preprint arXiv:2010.11929. 2020.
- [45] D. Dreizin, Y. Zhou, Y. Zhang, N. Tirada, and A. L. Yuille. “Performance of a Deep Learning Algorithm for Automated Segmentation and Quantification of Traumatic Pelvic Hematomas on CT”. In: *Journal of Digital Imaging* (2019), pp. 1–9.

- [46] M. El Adoui, S. A. Mahmoudi, M. A. Larhman, and M. Benjelloun. “MRI Breast Tumor Segmentation Using Different Encoder and Decoder CNN Architectures”. In: *Computers* 8 (2018), pp. 52–63.
- [47] Mohammed El Adoui, Stylianos Drisis, and Mohammed Benjelloun. “Multi-Input Deep Learning Architecture for Predicting Breast Tumor Response to Chemotherapy Using Quantitative MR Images”. In: *International Journal of Computer Assisted Radiology and Surgery* 15 (2020), pp. 1491–1500.
- [48] W. Eziddin. “Segmentation Itérative d’Images par Propagation de Connaissances dans le Domaine Possibiliste: Application à la Détection de Tumeurs en Imagerie Mammographique”. PhD thesis. Université Européenne de Bretagne, Brest, France, June 2012.
- [49] H. Fan, C. Zhang, K. Zhang, and R. Yao. “An Improved CV Model for Breast MR Images Segmentation”. In: *International Conference on Bioinformatics and Biomedicine*. IEEE, 2018, pp. 2243–2248.
- [50] A. Q. Al-Faris, U. K. Ngah, N. A. M. Isa, and I. L. Shuaib. “Computer-Aided Segmentation System for Breast MRI Tumour Using Modified Automatic Seeded Region Growing”. In: *Journal of Digital Imaging* 27 (2014), pp. 133–144.
- [51] O. Favaron, G. Fricke, W. Goddard, S. M. Hedetniemi, S. T. Hedetniemi, P. Kristiansen, R. C. Laskar, and R. D. Skaggs. “Offensive Alliances in Graphs”. In: *Discussiones Mathematicae Graph Theory* 24.2 (2004), pp. 263–275.
- [52] P. F. Felzenszwalb and D. P. Huttenlocher. “Efficient Graph-Based Image Segmentation”. In: *International Journal of Computer Vision* 59 (2004).
- [53] E. Fix and J. L. Hodges Jr. “Discriminatory Analysis-Nonparametric Discrimination: Consistency Properties”. In: *Technical Report, Randolph Field Texas: U.S. Air Force School of Aviation Medicine* (1951).
- [54] G. W. Flake, S. Lawrence, and C. L. Giles. “Efficient Identification of Web Communities”. In: *Proceedings of the 6th ACM SIGKDD International Conference on Knowledge Discovery and Data Mining (KDD-2000)*. 2000, pp. 150–160.
- [55] G. H. Fricke, L. M. Lawson, T. W. Haynes, S. M. Hedetniemi, and S. T. Hedetniemi. “A Note on Defensive Alliances in Graphs”. In: *Bulletin of the Institute of Combinatorics and Its Applications* 38 (2003), pp. 37–41.
- [56] C. Gallego-Ortiz and A. L. Martel. “A Graph-Based Lesion Characterization and Deep Embedding Approach for Improved Computer-Aided Diagnosis of Nonmass Breast MRI Lesions”. In: *Medical Image Analysis* 51 (2019), pp. 116–124.
- [57] C. Gallego-Ortiz and A.L. Martel. “A graph-based lesion characterization and deep embedding approach for improved computer-aided diagnosis of nonmass breast MRI lesions”. In: *Medical Image Analysis* 51 (2019), pp. 116–124.
- [58] A. Garcia-Garcia, S. Orts-Escolano, S. Oprea, V. Villena-Martinez, P. Martinez-Gonzalez, and J. Garcia-Rodriguez. “A Survey on Deep Learning Techniques for Image and Video Semantic Segmentation”. In: *Applied Soft Computing* 70 (2018), pp. 41–65.
- [59] P. Ghamisi, M. S. Couceiro, F. M. L. Martins, and J. A. Benediktsson. “Multilevel Image Segmentation Based on Fractional-Order Darwinian Particle Swarm Optimization”. In: *IEEE Transactions on Geoscience and Remote Sensing* 52 (2013), pp. 2382–2394.

- [60] <https://gco.iarc.fr>. (Accessed : 24/06/2025).
- [61] A. B. de Gonzalez and S. Darby. “Risk of Cancer from Diagnostic X-rays: Estimates for the UK and 14 Other Countries”. In: *The Lancet* 363 (2004), pp. 345–351.
- [62] J. Gordillo, E. Montseny, and S. Sobrevilla. “State of the Art Survey on MRI Brain Tumor Segmentation”. In: *Magnetic Resonance Imaging* 31 (2013), pp. 1426–1438.
- [63] M. Ham and A. Moon. “Inflammatory and Microenvironmental Factors Involved in Breast Cancer Progression”. In: *Archives of Pharmacal Research* 36 (2013), pp. 1419–1431.
- [64] A. E. Hassanien, H. M. Moftah, A. T. Azar, and M. Shoman. “MRI Breast Cancer Diagnosis Hybrid Approach Using Adaptive Ant-Based Segmentation and Multilayer Perceptron Neural Networks Classifier”. In: *Applied Soft Computing* 14 (2014), pp. 62–71.
- [65] T. W. Haynes, S. T. Hedetniemi, and M. A. Henning. “Global Defensive Alliances in Graphs”. In: *Electronic Journal of Combinatorics* 10 (2003), R47.
- [66] K. He, X. Zhang, S. Ren, and J. Sun. “Deep Residual Learning for Image Recognition”. In: *Proceedings of the IEEE Conference on Computer Vision and Pattern Recognition (CVPR)*. June 2016.
- [67] T. He, J. Song, Y. Zhu, J. Wang, G. Huang, Y. Qiao, and J. Sun. “Parametric Noise Injection: Trainable Randomness to Improve Deep Neural Network Robustness Against Adversarial Attack”. In: *Proceedings of the IEEE/CVF Conference on Computer Vision and Pattern Recognition (CVPR)*. 2020, pp. 588–597.
- [68] D. Hendrycks, M. Mazeika, S. Kadavath, and D. Song. “Many Faces of Robustness: A Critical Analysis of Out-of-Distribution Generalization”. In: *International Conference on Machine Learning (ICML)*. 2020, pp. 2751–2769.
- [69] T. Herman. *Fundamentals of Computerized Tomography: Image Reconstruction from Projections*. 2nd. London: Springer Science and Business Media, 2009.
- [70] Lukas Hirsch, Yu Huang, Shaojun Luo, Carolina Rossi Saccarelli, Roberto Lo Gullo, Isaac Daimiel Naranjo, A. G. Bitencourt, Natsuko Onishi, Eun Sook Ko, Dortis Leithner, et al. “Deep Learning Achieves Radiologist-Level Performance of Tumor Segmentation in Breast MRI”. In: *ArXiv:2009.09827 Phys. Stat.* (2020).
- [71] M. Hmida, K. Hamrouni, B. Solaiman, and S. Boussetta. “Mammographic mass segmentation using fuzzy contours”. In: *Computer Methods and Programs in Biomedicine* 164 (2018), pp. 131–142.
- [72] S. L. Horowitz and T. Pavlidis. “Picture Segmentation by a Tree Traversal Algorithm”. In: *Journal of the ACM* 23 (1976), pp. 368–388.
- [73] B. Huang, M. Warner, and J. A. Gustafsson. “Estrogen Receptors in Breast Carcinogenesis and Endocrine Therapy”. In: *Molecular and Cellular Endocrinology* (2015), pp. 240–244.
- [74] B. Huang, M. Warner, and J. A. Gustafsson. “Estrogen Receptors in Breast Carcinogenesis and Endocrine Therapy”. In: *Molecular and Cellular Endocrinology* 418 (2015), pp. 240–244.
- [75] K. M. Iftekharuddin, J. Zheng, M. A. Islam, and R. J. Ogg. “Fractal-Based Brain Tumor Detection in Multimodal MRI”. In: *Applied Mathematics and Computation* 207 (2009), pp. 23–41.

- [76] *IRM Diffusion (Vidéo)*. <https://www.cea.fr/multimedia/pages/videos/culture-scientifique/sante-sciences-du-vivant/video-irm-diffusion.aspx>. (Accessed : 24/06/2025).
- [77] A. Israel. “Breast Cancer: The Past, the Present, and a Look Towards the Future”. PhD thesis in Biology. University of Yeshiva, New York, June 2019.
- [78] R. Jain and R. S. Sharma. “Image Segmentation Through Fuzzy Clustering: A Survey”. In: *Harmony Search and Nature Inspired Optimization Algorithm*. Ed. by N. Yadav, A. Yadav, J. C. Bansal, K. Deep, and J. H. Kim. 1st. Singapore: Springer, 2019, pp. 497–508.
- [79] J. Jayender, S. Chikarmane, F. A. Jolesz, and E. Gombos. “Automatic Segmentation of Invasive Breast Carcinomas from Dynamic Contrast-Enhanced MRI Using Time Series Analysis”. In: *Journal of Magnetic Resonance Imaging* 79.5 (2014), pp. 467–475.
- [80] J. S. Jeyanathan, A. Shenbagavalli, B. Venkatraman, and M. Menaka. “Analysis of Breast Thermograms in Lateral Views Using Texture Features”. In: *IEEE TENCON 2018-2018 IEEE Region 10 Conference*. 2018, pp. 2017–2022.
- [81] Han Jiao, Xinhua Jiang, Zhiyong Pang, Xiaofeng Lin, Yihua Huang, and Li Li. “Deep Convolutional Neural Networks-Based Automatic Breast Segmentation and Mass Detection in DCE-MRI”. In: *Computational and Mathematical Methods in Medicine* 2020.1 (2020), p. 2413706.
- [82] F. Jie, Y. Shi, Y. Li, and Z. Liu. “Interactive Region-Based MRF Image Segmentation”. In: *4th International Congress on Image and Signal Processing - IEEE*. 2011, pp. 1263–1267.
- [83] C. T. Johnston, K. T. Gribbon, and D. G. Bailey. “Implementing Image Processing Algorithms on FPGAs”. In: *11th Electronics New Zealand Conference*. 2004, pp. 118–123.
- [84] *Introduction to Image Segmentation with K-Means Clustering*. <https://www.kdnuggets.com/2019/08/introduction-image-segmentation-k-means-clustering.html>. (Accessed : 24/06/2025).
- [85] M. Kass, A. Witkin, and D. Terzopoulos. “Snakes: Active Contour Models”. In: *International Journal of Computer Vision* 1 (1988), pp. 321–331.
- [86] H. Khastavaneh and H. Haron. “A Conceptual Model for Segmentation of Multiple Sclerose Lesions in Magnetic Resonance Images Using Massive Training Artificial Neural Network”. In: *5th International Conference on Intelligent Systems, Modelling and Simulation*. IEEE, 2014, pp. 273–278.
- [87] D. Kim, M. Park, J. Lee, H. B. Kim, and H. Kim. “Structured Noise Injection for Deep Learning Regularization”. In: *Proceedings of the 30th ACM International Conference on Information & Knowledge Management (CIKM)*. 2021, pp. 1645–1654.
- [88] Alex Krizhevsky, Ilya Sutskever, and Geoffrey E. Hinton. “ImageNet Classification with Deep Convolutional Neural Networks”. In: *Advances in Neural Information Processing Systems*. 2012, pp. 1097–1105.
- [89] C. K. Kuhl, H. B. Bieling, J. Gieseke, B. P. Kreft, T. Sommer, G. Lutterbey, and H. H. Schild. “Healthy Premenopausal Breast Parenchyma in Dynamic Contrast-Enhanced MR Imaging of the Breast: Normal Contrast Medium Enhancement and Cyclical-Phase Dependency”. In: *Radiology* 215.1 (2000), pp. 153–161.

- [90] C. K. Kuhl, S. Schrading, C. C. Leutner, N. Morakkabati-Spitz, E. Wardelmann, R. Fimmers, W. Kuhn, and H. H. Schild. “Mammography, Breast Ultrasound, and Magnetic Resonance Imaging for Surveillance of Women at High Familial Risk for Breast Cancer”. In: *Journal of Clinical Oncology* 23.33 (2005), pp. 8469–8476.
- [91] Christiane K. Kuhl, Simone Schrading, Claudia C. Leutner, Nuschin Morakkabati-Spitz, Eva Wardelmann, Rolf Fimmers, Walther Kuhn, and Hans H. Schild. “Mammography, Breast Ultrasound, and Magnetic Resonance Imaging for Surveillance of Women at High Familial Risk for Breast Cancer”. In: *Journal of Clinical Oncology* 23.33 (2005), pp. 8469–8476.
- [92] P. C. Lauterbur. “Image Formation by Induced Local Interactions: Examples Employing Nuclear Magnetic Resonance”. In: *Nature* 242 (1973), pp. 190–191.
- [93] P. C. Lauterbur. “Image Formation by Induced Local Interactions: Examples Employing Nuclear Magnetic Resonance”. In: *Nature* 242.5394 (1973), pp. 190–191.
- [94] Yann LeCun, Yoshua Bengio, and Geoffrey Hinton. “Deep Learning”. In: *Nature* 521.7553 (2015), pp. 436–444.
- [95] Yann LeCun, Léon Bottou, Yoshua Bengio, and Patrick Haffner. “Gradient-Based Learning Applied to Document Recognition”. In: *Proceedings of the IEEE* 86.11 (1998), pp. 2278–2324.
- [96] B. D. Lee, K. C. Liu, S. F. Hung, P. C. Lei, T. L. Wang, and Yang. “Breast Tumor Classification of Ultrasound Images Using Wavelet-Based Channel Energy and Images”. In: *Journal of Selected Topics in Signal Processing* 3 (2009), pp. 81–93.
- [97] S. Lee, Q. Huang, L. Jin, M. Lu, and T. Wang. “A Graph-Based Segmentation Method for Breast Tumors in Ultrasound Images”. In: *4th International Conference on Bioinformatics and Biomedical Engineering*. IEEE, 2010, pp. 1–4.
- [98] I. Leichter, Z. Gallimidi, A. Heyman-Reiss, N. Merlet, E. Ratner, M. Abramov, I. Stainvas, and R. Lederman. “Is CAD able to assist in the detection of subtle breast findings-lobular cancers, and t1a/t1b masses in dense breasts?”. In: *International Workshop on Digital Mammography*. Springer. 2010, pp. 474–480.
- [99] D. Levi, N. Ben-Zrihem, and E. Fetaya. “Structured Noise Injection for Regularization in Deep Neural Networks”. In: *International Conference on Learning Representations (ICLR)*. 2021.
- [100] C. Li, R. Huang, Z. Ding, J. Gatenby, D. N. Metaxas, and J. C. Gore. “A Level Set Method for Image Segmentation in the Presence of Intensity Inhomogeneities with Application to MRI”. In: *IEEE Transactions on Image Processing* 20 (2011), pp. 2007–2016.
- [101] G. Litjens, T. Kooi, B. E. Bejnordi, et al. “A Survey on Deep Learning in Medical Image Analysis”. In: *Medical Image Analysis* 42 (2017), pp. 60–88.
- [102] G. Litjens, T. Kooi, B. E. Bejnordi, et al. “A Survey on Deep Learning in Medical Image Analysis”. In: *Medical Image Analysis* 42 (2017), pp. 60–88.
- [103] G. Litjens, T. Kooi, B. E. Bejnordi, et al. “A Survey on Deep Learning in Medical Image Analysis”. In: *Medical Image Analysis* 42 (2017), pp. 60–88.

- [104] Geert Litjens, Thijs Kooi, Babak E. Bejnordi, Arnaud A. A. Setio, Francesco Ciompi, Mohsen Ghafoorian, Jeroen A. W. M. van der Laak, Bram Ginneken, and Clara I. Sánchez. “A Survey on Deep Learning in Medical Image Analysis”. In: *Medical Image Analysis* 42 (2017), pp. 60–88.
- [105] Gengbo Liu, Debasis Mitra, Ella F. Jones, Benjamin L. Franc, Spencer C. Behr, Alex Nguyen, Marjan S. Bolouri, Dorota J. Wisner, Bonnie N. Joe, Laura J. Esserman, et al. “Mask-Guided Convolutional Neural Network for Breast Tumor Prognostic Outcome Prediction on 3D DCE-MR Images”. In: *Journal of Digital Imaging* 34 (2021), pp. 630–636.
- [106] Z. Liu, Y. Lin, Y. Cao, et al. “Swin Transformer: Hierarchical Vision Transformer Using Shifted Windows”. In: *Proceedings of the IEEE International Conference on Computer Vision (ICCV)*. 2021, pp. 10012–10022.
- [107] M. Lobbes, M. Smidt, K. Keymeulen, R. Girometti, C. Zuiani, R. Beets-Tan, J. Wildberger, and C. Boetes. “Malignant Lesions on Mammography: Accuracy of Two Different Computer-Aided Detection Systems”. In: *Clinical Imaging* 37 (2013), pp. 283–288.
- [108] M. Lobbes, M. Smidt, K. Keymeulen, R. Girometti, C. Zuiani, R. Beets-Tan, J. Wildberger, and C. Boetes. “Malignant Lesions on Mammography: Accuracy of Two Different Computer-Aided Detection Systems”. In: *Clinical Imaging* 37 (2013), pp. 283–288.
- [109] M. Lobbes, M. Smidt, K. Keymeulen, R. Girometti, C. Zuiani, R. Beets-Tan, J. Wildberger, and C. Boetes. “Malignant lesions on mammography: accuracy of two different computer-aided detection systems”. In: *Clinical Imaging* 37 (2013), pp. 283–288.
- [110] J. Long, E. Shelhamer, and T. Darrell. “Fully Convolutional Networks for Semantic Segmentation”. In: *Conference on Computer Vision and Pattern Recognition*. IEEE, 2015, pp. 3431–3440.
- [111] S. Madhukumara and N. Santhiyakumari. “Evaluation of K-Means and Fuzzy C-Means Segmentation on MR Images of Brain”. In: *The Egyptian Journal of Radiology and Nuclear Medicine* 46 (2015), pp. 475–479.
- [112] M. Maeda and S. Tsuda. “Reduction of Artificial Bee Colony Algorithm for Global Optimization”. In: *Neurocomputing* 148 (2015), pp. 70–74.
- [113] G. Maicas, G. Carneiro, and A. P. Bradley. “Globally Optimal Breast Mass Segmentation from DCE-MRI Using Deep Semantic Segmentation as Shape Prior”. In: *14th International Symposium on Biomedical Imaging*. IEEE, 2017, pp. 305–309.
- [114] P. Mansfield. “Multi-Planar Image Formation Using NMR Spin Echoes”. In: *Journal of Physics C: Solid State Physics* 10.3 (1977), pp. L55–L58.
- [115] N. Maouche and J. Oudia. “Approche à Base d’Alliances dans les Graphes pour la Réduction de la Congestion dans les VANETs”. MA thesis. Département d’Informatique, Université de Béjaia, Juillet 2017.
- [116] D. Marr and E. Hildreth. “Theory of Edge Detection”. In: *In 4th International Congress on Image and Signal Processing - Series B. Biological Sciences* 207 (1980), pp. 187–217.
- [117] *Mastectomy (Definition)*. <https://www.cancer.gov/publications/dictionaries/cancer-terms/def/mastectomy>. (Accessed : 24/06/2025).
- [118] D. McClymont, A. Mehnert, A. Trakic, D. Kennedy, and S. Crozier. “Fully Automatic Lesion Segmentation in Breast MRI Using Mean-Shift and Graph-Cuts on a Region Adjacency Graph”. In: *Journal of Magnetic Resonance Imaging* 39 (2014), pp. 795–804.

- [119] S. Miah, C. A. Banks, M. K. Adams, L. Florens, K. E. Lukong, and M. P. Washburn. “Advancement of Mass Spectrometry-Based Proteomics Technologies to Explore Triple Negative Breast Cancer”. In: *Molecular BioSystems* (2017).
- [120] S. Michahial and B. A. Thomas. “Applying Cuckoo Search Based Algorithm and Hybrid Based Neural Classifier for Breast Cancer Detection Using Ultrasound Images”. In: *Evolutionary Intelligence* (2019), pp. 1–18.
- [121] H. M. Moftah, A. T. Azar, E. T. Al-Shammari, N. I. Ghali, A. E. Hassanien, and M. Shoman. “Adaptive K-Means Clustering Algorithm for MR Breast Image Segmentation”. In: *Neural Computing and Applications* 24 (2014), pp. 1917–1928.
- [122] K. Mori, N. Niki, Y. Kawata, H. Fujita, M. Oda, H. Kim, H. Arimura, A. Shimizu, S. Noriki, K. Inai, and H. Kimura. “Applied Technologies and Systems”. In: *Computational Anatomy Based on Whole Body Imaging*. Ed. by K. Hidefumi and M. Yoshitaka. 1st. Tokyo: Springer, 2017, pp. 285–352.
- [123] E. Mortensen. “Interactive Segmentation with Intelligent Scissors”. In: *Graphical Models and Image Processing* 60 (1998), pp. 349–384.
- [124] C. K. Mummadi, M. Rosendahl, T. Brox, and V. Natarajan. “On the Robustness of Semantic Segmentation Models to Input Perturbations”. In: *Proceedings of the IEEE/CVF Conference on Computer Vision and Pattern Recognition (CVPR)*. 2021, pp. 888–897.
- [125] J. Nahla and M. Monica. “Application of Fuzzy Neural Network for Image Tumor Description”. In: *World Academy of Science, Engineering and Technology* (2019).
- [126] A. Nakib, B. Daachi, and P. Siarry. “Hybrid Differential Evolution Using Low-Discrepancy Sequences for Image Segmentation”. In: *26th International Parallel and Distributed Processing Symposium Workshops and PhD Forum*. IEEE, 2012, pp. 634–640.
- [127] A. Nakib, H. Oulhadj, and P. Siarry. “Image Histogram Thresholding Based on Multi-Objective Optimization”. In: *Signal Processing* 87 (2007), pp. 2516–2534.
- [128] N.Q. Nguyen and S.W. Lee. “Robust Boundary Segmentation in Medical Images Using a Consecutive Deep Encoder-Decoder Network”. In: *IEEE Access* 7 (2019), pp. 33795–33808.
- [129] C. F. Nodine and H. L. Kundel. “Using Eye Movements to Study Visual Search and to Improve Tumor Detection”. In: *Radiographics: A Review Publication of the Radiological Society of North America, Inc* 7 (1987), pp. 1241–1250.
- [130] C. F. Nodine and H. L. Kundel. “Using eye movements to study visual search and to improve tumor detection”. In: *Radiographics : a review publication of the Radiological Society of North America, Inc* 7 (1987), pp. 1241–1250.
- [131] P. Orbanz and J. M. Buhmann. “Nonparametric Bayesian Image Segmentation”. In: *Journal of Magnetic Resonance Imaging* 77 (2008), pp. 25–45.
- [132] <https://www.who.int/>. (Accessed : 24/06/2025).
- [133] S. Osher and J. A. Sethian. “Fronts Propagating with Curvature-Dependent Speed: Algorithms Based on Hamilton-Jacobi Formulations”. In: *Journal of Computational Physics* 79 (1988), pp. 12–49.
- [134] K. Ouazine. “Alliances dans les Graphes: Propriétés et Application pour la Réduction de la Saturation et de la Congestion dans les Réseaux VANETs”. Thèse en Informatique. Université de Béjaia, Août 2018.

- [135] K. Ouazine, H. Slimani, H. Nacer, N. Bermad, and S. Zemmoudj. “Reducing Saturation and Congestion in VANET Networks: Alliance-Based Approach and Comparisons”. In: *International Journal of Communication Systems* 33.4 (2020), e4245.
- [136] K. Ouazine, H. Slimani, H. Nacer, J. Oudia, and N. Maouche. “Alliance Based Approach for Reducing Saturation and Congestion in VANETs”. In: *2018 International Symposium on Programming and Systems (ISPS)*. 2018, pp. 1–6.
- [137] G. Pavlidis. *Segmentation of Digital Images*. Signals and Communication Technology. Springer, 2017, pp. 213–260.
- [138] B. Peng, L. Zhang, and D. Zhang. “A Survey of Graph Theoretical Approaches to Image Segmentation”. In: *Pattern Recognition* 46 (2013), pp. 1020–1038.
- [139] Chengtao Peng, Yue Zhang, Jian Zheng, Bin Li, Jun Shen, Ming Li, Lei Liu, Bensheng Qiu, and Danny Z Chen. “IMIIN: An Inter-Modality Information Interaction Network for 3D Multi-Modal Breast Tumor Segmentation”. In: *Computerized Medical Imaging and Graphics* 95 (2022), p. 102021.
- [140] G. Piantadosi. “Pattern Recognition in Breast DCE-MRI Automatic Cancer Analysis”. PhD thesis. Università Degli Studi Di Napoli Federico II, Napoli, Italy, June 2018.
- [141] E. J. Pruche and K. Bellenir. *Breast Cancer Sourcebook (Health Reference Series)*. Omni-graphics, 2001.
- [142] *Python (Langage de Programmation) - Wikipédia*. [https://fr.wikipedia.org/wiki/Python_\(langage\)](https://fr.wikipedia.org/wiki/Python_(langage)). (Accessed : 24/06/2025).
- [143] S. Rahangdale, P. Keijzer, and P. Kruit. “MBSEM Image Acquisition and Image Processing in LabView FPGA”. In: *International Conference on Systems, Signals and Image Processing, IEEE*. 2016, pp. 1–4.
- [144] N. S. M. Raja, S. L. Fernandes, N. Dey, S. C. Satapathy, and V. Rajinikanth. “Contrast Enhanced Medical MRI Evaluation Using Tsallis Entropy and Region Growing Segmentation”. In: *Journal of Ambient Intelligence and Humanized Computing* (2018), pp. 1–12.
- [145] N. K. Raman and N. Sahu. “Efficient System for Devanagari Script Segmentation”. In: *2nd International Conference on Computing for Sustainable Global Development - IEEE*. 2015, pp. 722–725.
- [146] N. V. Rehman, J. Wang, H. Weiyang, I. Ali, A. Akbar, M. Assam, Y. Ghadi Yasin, and A. Algarni. “Edge of Discovery: Enhancing Breast Tumor MRI Analysis with Boundary-Driven Deep Learning”. In: *Biomedical Signal Processing and Control* 95 (2024), p. 106291.
- [147] *RIDER Breast MRI (Dataset)*. <https://wiki.cancerimagingarchive.net/display/Public/RIDER+Breast+MRI>. (Accessed : 24/06/2025).
- [148] L. G. Roberts. “Machine Perception of Three-Dimensional Solids”. PhD thesis. Massachusetts Institute of Technology, Cambridge, USA, June 1963.
- [149] O. Ronneberger, P. Fischer, and T. Brox. “U-net: Convolutional Networks for Biomedical Image Segmentation”. In: *International Conference on Medical Image Computing and Computer-Assisted Intervention*. Springer. 2015, pp. 234–241.
- [150] O. Ronneberger, Philipp Fischer, and Thomas Brox. “U-net: Convolutional Networks for Biomedical Image Segmentation”. In: *Medical Image Computing and Computer-Assisted Intervention. MICCAI 2015: 18th International Conference, Proceedings, Part III*. Vol. 18. 2015.

- [151] Olaf Ronneberger, Philipp Fischer, and Thomas Brox. “U-net: Convolutional Networks for Biomedical Image Segmentation”. In: *International Conference on Medical Image Computing and Computer-Assisted Intervention*. Springer, 2015, pp. 234–241.
- [152] K. R. Sail. “Outcomes Associated with Chemotherapy in Elderly Patients with Early Stage Operable Breast Cancer”. PhD thesis in Health Science. The University of Texas, Texas, USA, Aug. 2010.
- [153] L. Sani, M. Paoli, G. Raspa, A. Vispa, N. Ghavami, G. Tiberi, A. Saracini, S. Ercolani, E. Vannini, and M. Duranti. “Microwave Apparatus for Testing Breast Integrity Based on Huygens’ Principle: Clinical Validation on 16 Subjects”. In: *Loughborough Antennas and Propagation Conference*. Ed. by IET Digital Library. 2017, pp. 1–5.
- [154] <https://www.e-cancer.fr/Patients-et-proches/Les-cancers/Cancer-du-sein/Anatomie-du-sein>. (Accessed : 24/06/2025).
- [155] M. Semchedine. “Contribution à la Segmentation d’Images Médicales par les Algorithmes Bio-Inspirés”. PhD thesis in Computer Science. Université Ferhat Abbas de Sétif, Juillet 2018.
- [156] J. Senthilnath, R. Rajendra, S. Suresh, S. Kulkarni, and J. A. Benediktsson. “Hierarchical Clustering Approaches for Flood Assessment Using Multi-Sensor Satellite Images”. In: *International Journal of Image and Data Fusion* 10 (2019), pp. 28–44.
- [157] K. H. Shafique and R. D. Dutton. “A Tight Bound on the Cardinalities of Maximum Alliance-Free and Minimum Alliance-Cover Sets”. In: *Journal of Combinatorial Mathematics and Combinatorial Computing* 10 (2006), pp. 139–145.
- [158] A. Sharifian, S. F. Sasansara, M. J. Ghadi, S. Ghavidel, L. Li, and J. Zhang. “Dynamic Performance Improvement of an Ultra-Lift Luo DC-DC Converter by Using a Type-2 Fuzzy Neural Controller”. In: *Computers and Electrical Engineering* 69 (2018), pp. 171–182.
- [159] J. Shi and J. Malik. “Normalized Cuts and Image Segmentation”. In: *IEEE Transactions on Pattern Analysis and Machine Intelligence* 22 (2000), pp. 888–905.
- [160] T. Si, D. K. Patra, S. Mondal, and P. Mukherjee. “Breast Lesion Segmentation in DCE-MRI Using Multi-Objective Clustering with NSGA-II”. In: *International Conference on Innovative Trends in Information Technology (ICITIIT)*. IEEE, 2022.
- [161] I. Sobel and G. Feldman. “A 3x3 Isotropic Gradient Operator for Image Processing”. In: *Presented as a Talk Within the Stanford Artificial Intelligence Project* (1968).
- [162] <https://pathology.jhu.edu/breast/staging-grade/>. (Accessed : 24/06/2025).
- [163] L. Sun, J. He, X. Yin, Y. Zhang, J. H. Chen, T. Kron, and M. Y. Su. “An Image Segmentation Framework for Extracting Tumors from Breast Magnetic Resonance Images”. In: *Journal of Innovative Optical Health Sciences* 11 (2018), pp. 1850014–1850015.
- [164] G. Szabö and T. Czàrà̀n. “Defensive Alliances in Spatial Models of Cyclical Population Interactions”. In: *Physical Reviews* 64 (2001), 11 pages.
- [165] <https://acsjournals.onlinelibrary.wiley.com/doi/10.3322/caac.21834>. (Accessed : 24/06/2025).
- [166] A. Teramoto, S. Miyajo, H. Fujita, O. Yamamuro, K. Omi, and M. Nishio. “Automated Analysis of Breast Tumour in the Breast DCE-MR Images Using Level Set Method and Selective Enhancement of Invasive Regions”. In: *International Workshop on Breast Imaging*. Springer, 2016, pp. 439–445.

- [167] B. Thapa, S. Thapa, S. P. Aryal, A. Sedhain, and A. Shrestha. “Performance Evaluation of CNN Under Different Types of Noise for Augmented Medical Image Classification”. In: *Procedia Computer Science* 179 (2021), pp. 524–531.
- [168] *TSA-Algérie: Il y a Deux Types de Cancers qui se Détachent en Algérie*. <https://www.tsa-algerie.com/pr-zitouni-il-y-a-deux-types-de-cancers-qui-se-detachent-en-algerie/>. (Accessed: 24/06/2025).
- [169] V. Vapnik. *The Nature of Statistical Learning Theory*. 1st. New York: Springer Science and Business Media, 1995, pp. 213–260.
- [170] A. Vaswani, N. Shazeer, N. Parmar, et al. “Attention is All You Need”. In: *Advances in Neural Information Processing Systems (NeurIPS)*. Vol. 30. 2017, pp. 5998–6008.
- [171] U. Veronesi, B. Salvadori, A. Luini, M. Greco, R. Saccozzi, M. Del Vecchio, L. Mariani, S. Zurrida, and F. Rilke. “Breast Conservation Is a Safe Method in Patients with Small Cancer of the Breast. Long-Term Results of Three Randomised Trials on 1.973 Patients”. In: *European Journal of Cancer* 31 (1995), pp. 1574–1579.
- [172] Hongyu Wang, Jiaqi Cao, Jun Feng, Yilin Xie, Di Yang, and Baoying Chen. “Mixed 2D and 3D Convolutional Network with Multi-Scale Context for Lesion Segmentation in Breast DCE-MRI”. In: *Biomedical Signal Processing and Control* 68 (2021), p. 102607.
- [173] Z. Wang, J. R. Jensen, and J. Im. “An Automatic Region-Based Image Segmentation Algorithm for Remote Sensing Applications”. In: *Environmental Modelling and Software* 25 (2010), pp. 1149–1165.
- [174] <https://fr.wikipedia.org/wiki/Sein>. (Accessed : 24/06/2025).
- [175] Z. Wu and R. Leahy. “An Optimal Graph Theoretic Approach to Data Clustering: Theory and Its Application to Image Segmentation”. In: *IEEE Transactions on Pattern Analysis and Machine Intelligence* 15 (2002), pp. 1101–1113.
- [176] E. Xie, W. Wang, Z. Yu, et al. “SegFormer: Simple and Efficient Design for Semantic Segmentation with Transformers”. In: *Advances in Neural Information Processing Systems (NeurIPS)*. Vol. 34. 2021, pp. 12077–12090.
- [177] X. Xie, S. Y. Yeo, M. Mirmehdi, I. Sazonov, and P. Nithiarasu. “Image Gradient Based Level Set Methods in 2D and 3D”. In: *Deformation Models*. Ed. by H. M. González, A. M. Torres, and J. V. Gómez. 1st. Dordrecht: Springer, 2013, pp. 101–120.
- [178] Y. Xu and E. C. Uberbacher. “2D Image Segmentation Using Minimum Spanning Trees”. In: *Image and Vision Computing* 15 (1997), pp. 47–57.
- [179] Z. Xu and P. K. Srimani. “Self-Stabilizing Distributed Algorithms for Graph Alliances”. In: *Proceedings of the 20th International Parallel and Distributed Processing Symposium* (2006).
- [180] F. Yang and T. Jiang. “Pixon-Based Image Segmentation with Markov Random Fields”. In: *IEEE Transactions on Image Processing* 12.12 (2003), pp. 1552–1559.
- [181] J. Yao, J. Chen, and C. Chow. “Breast Tumor Analysis in Dynamic Contrast Enhanced MRI Using Texture Features and Wavelet Transform”. In: *IEEE Journal of Selected Topics in Signal Processing* 3 (2009), pp. 94–100.
- [182] I. G. Yero and J. A. Rodríguez-Velázquez. “Boundary Powerful K-Alliances in Graphs”. In: *Ars Combinatoria* 111 (2013), pp. 495–504.

- [183] H. Young, R. Baum, U. Cremerius, K. Herholz, O. Hoekstra, A. A. Lammertsma, J. Pruim, and P. Price. “Measurement of Clinical and Subclinical Tumor Response Using [18F]-Fluorodeoxyglucose and Positron Emission Tomography: Review and 1999 EORTC Recommendations”. In: *European Journal of Cancer* 35 (1999), pp. 1773–1782.
- [184] N. Yu, J. Wu, S. P. Weinstein, B. Gaonkar, B. M. Keller, A. B. Ashraf, Y. Jiang, C. Davatzikos, E. F. Conant, and D. Kontos. “A Superpixel-Based Framework for Automatic Tumor Segmentation on Breast DCE-MRI”. In: *Medical Imaging 2015: Computer-Aided Diagnosis*. International Society for Optics and Photonics, 2015, 941400.
- [185] Q. Yu, K. Huang, Y. Zhu, X. Chen, and W. Meng. “Preliminary results of computer-aided diagnosis for magnetic resonance imaging of solid breast lesions”. In: *Breast Cancer Research and Treatment*. Springer, 2019.
- [186] A. H. Yurttakal, H. Erbay, T. Ikizceli, and S. Karacavus. “Detection of Breast Cancer Via Deep Convolution Neural Networks Using MRI Images”. In: *Multimedia Tools and Applications* 79.5 (2020).
- [187] C. T. Zahn. “Graph-Theoretical Methods for Detecting and Describing Gestalt Clusters”. In: *IEEE Transactions on Computers* 1 (1971), pp. 68–86.
- [188] *National Cancer Institute (Official Website)*. <https://www.cancer.gov/>. (Accessed : 24/06/2025).
- [189] *Anaconda Distribution*. <https://www.anaconda.com/products/distribution>. (Accessed : 24/06/2025).
- [190] Y. Zhang, S. Chan, V. Y. Park, K. Chang, S. Mehta, M. J. Kim, F. J. Combs, P. Chang, D. Chow, R. Parajuli, et al. “Automatic Detection and Segmentation of Breast Cancer on MRI Using Mask R-CNN Trained on Non-Fat-Sat Images and Tested on Fat-Sat Images”. In: *Academic Radiology* 29 (2022), S135–S144.
- [191] Y. Zhang, S. Li, V. Y. Park, K. T. Chang, S. Mehta, M. J. Kim, F. J. Combs, P. Chang, D. Chow, R. Parajuli, R. S. Mehta, C. Y. Lin, S. H. Chien, J. H. Chen, and M. Y. Su. “Automatic Detection and Segmentation of Breast Cancer on MRI Using Mask R-CNN Trained on Non Fat-Sat Images and Tested on Fat-Sat Images”. In: *Academic Radiology* (2020).
- [192] Y. Zhang, S. Li, Z. Xu, and J. Yuan. “Novel Approach for Region Merging and Image Segmentation for Human-Computer Interaction”. In: *Optical Engineering* 42 (2003), pp. 2277–2280.
- [193] S. Zhao, L. Zhang, Y. Shen, and Y. Zhu. “A CNN-Based Depth Estimation Approach with Multiscale Sub-Pixel Convolutions and a Smoothness Constraint”. In: *Asian Conference on Computer Vision*. Springer, 2018, pp. 365–380.
- [194] X. Zhao, Y. Liao, J. Xie, X. He, S. Zhang, G. Wang, J. Fang, H. Lu, and J. Yu. “BreastDM: A DCE-MRI Dataset for Breast Tumor Image Segmentation and Classification”. In: *Computers in Biology and Medicine* 164 (2023), p. 107255.
- [195] Z. Zhong, L. Zheng, G. Kang, S. Li, and Y. Yang. “Random Erasing Data Augmentation”. In: *Proceedings of the AAAI Conference on Artificial Intelligence*. Vol. 34. 07. 2020, pp. 13001–13008.

- [196] R. G. Ziegler, R. N. Hoover, M. C. Pike, A. Hildesheim, A. M. Nomura, D. W. West, A. H. Wu-Williams, L. N. Kolonel, P. L. Horn-Ross, J. F. Rosenthal, and M. B. Hyer. “Migration Patterns and Breast Cancer Risk in Asian-American Women”. In: *Journal of the National Cancer Institute* 85 (1993), pp. 1819–1827.

ABSTRACT

Breast cancer is one of the most common and deadly cancers in women. Furthermore, dynamic contrast-enhanced magnetic resonance imaging (DCE-MRI) plays a key role in its diagnosis. However, the images produced by this latter medical imaging modality are often affected by Rician noise, which badly affects the performance of segmentation models. This manuscript reviews and discusses recent deep learning methods for DCE-MRI breast tumor segmentation. Then, it introduces RicIU-Net, a U-Net variant that injects Rician noise into encoder layers during training to improve robustness. Tested on the public BreastDM dataset, RicIU-Net outperforms U-Net and U-Net 2.1D in terms of ice sore and yields a satisfactory IoU score, showing better adaptation to real-world imaging conditions. Hence, the proposed approach offers a simple yet effective way to enhance the reliability of the segmentation without external denoising.

Key words : Breast DCE-MRI; Tumor region; Image segmentation; U-Net architecture; Deep learning; Convolutional neural network.

RÉSUMÉ

Le cancer du sein est l'un des cancers les plus fréquents et les plus mortels chez la femme. L'imagerie par résonance magnétique avec injection de produit de contraste (IRM DCE) joue un rôle essentiel dans son diagnostic. Toutefois, les images produites par cette modalité d'imagerie médicale sont souvent affectées par le bruit de Rician, ce qui nuit fortement aux performances des modèles de segmentation. Ce mémoire passe en revue et analyse les méthodes récentes d'apprentissage profond pour la segmentation des tumeurs mammaires en IRM DCE. Il propose ensuite RicIU-Net, une variante de U-Net intégrant une injection contrôlée de bruit de Rician dans les couches de l'encodeur durant l'entraînement, afin d'améliorer la robustesse du modèle. Évalué sur la base de données publique BreastDM, RicIU-Net surpasse U-Net et U-Net 2.1D en termes de Dice score, et présente un score IoU satisfaisant, montrant une meilleure adaptation aux conditions d'imagerie réelles. Ainsi, l'approche proposée constitue une solution simple mais efficace pour renforcer la fiabilité de la segmentation sans recourir à un prétraitement externe.

Mots-clés : IRM mammaire DCE ; Région tumorale ; Segmentation d'images ; Architecture U-Net; Apprentissage profond ; Réseau de neurones convolutionnel.